Materials Horizons

REVIEW

View Article Online
View Journal

Cite this: DOI: 10.1039/c8mh01062e

Textile strain sensors: a review of the fabrication technologies, performance evaluation and applications

Shayan Seyedin, *[a] Peng Zhang,[a] Maryam Naebe,[a] Si Qin,[a] Jun Chen,[b] Xungai Wang[a] and Joselito M. Razal *[a]

The recent surge in using wearable personalized devices has made it increasingly important to have flexible textile-based sensor alternatives that can be comfortably worn and can sense a wide range of body strains. Typically fabricated from rigid materials such as metals or semiconductors, conventional strain sensors can only withstand small strains and result in bulky, inflexible, and hard-to-wear devices. Textile strain sensors offer a new generation of devices that combine strain sensing functionality with wearability and high stretchability. In this review, we discuss recent exciting advances in the fabrication, performance enhancement, and applications of wearable textile strain sensors. We describe conventional and novel approaches to achieve textile strain sensors such as coating, conducting elastomeric fiber spinning, wrapping, coiling, coaxial fiber processing, and knitting. We also discuss how important performance parameters such as electrical conductivity, mechanical properties, sensitivity, sensing range, and stability are influenced by fabrication strategies to illustrate their effects on the sensing mechanism of textile sensors. We summarize the potential applications of textile sensors in structural health monitoring, wearable body movement measurements, data gloves, and entertainment. Finally, we present the challenges and opportunities that exist to date in order to provide meaningful guidelines and directions for future research.

Received 31st August 2018,
Accepted 10th December 2018

DOI: 10.1039/c8mh01062e

rsc.li/materials-horizons

Introduction

Strain sensors are devices that can convert physical deformations into measurable signals.[1] Traditionally fabricated from metals or semiconductors to sense small deformations less than 5% strain, these devices are critical for structural health monitoring *i.e.* detecting material fatigue in bridges, airplanes, and rails.[2,3] The limited range of conventional strain sensors prohibits their use in wearable applications where deformation can be as large as 55%. These sensors are also inherently rigid and can be uncomfortable to wear. Recent advances in textile-based strain sensors show that new platform materials and technologies can be designed to suit large range sensing for use in wearable applications. Sports and recreational clothing that can track body movements[4–10] and fabrics that can assist in remote health monitoring,[11–14] virtual reality, and soft robotics[6] are some key demonstration applications to date.

Textile strain sensors can be made by coating conductive components onto existing fabrics. While simple to fabricate, these coated fabrics typically perform poorly during large mechanical deformations due to the damage in conductive circuits. An emerging alternative is to directly make elastomeric conductive filaments or yarns and then knit or weave them into a textile.[9,15–20] These filaments and yarns are realized by the recent advances in scalable fiber spinning technologies including wet-spinning. Also gaining traction is the geometrical manipulation of yarns by helically winding carbon nanotube (CNT) sheets onto a host template to make hierarchically buckled CNT coatings.[21,22] These new types of elastomeric fibers can sense strains as large as 600%.

With these recent advances, this review aims to provide valuable guidelines for the fabrication of sensitive and wearable textile strain sensors. The different evaluation methods of sensing performance are explained to elucidate how each exciting development fits into the field of wearable textile strain sensors. Fiber and textile characteristics affecting performance such as electrical and mechanical properties, sensitivity, sensing range, stability, and wearability are discussed and some metrics are presented to quantify these properties. The recent developments on fabrication technologies of strain sensing fibers,

[a] Deakin University, Institute for Frontier Materials, Geelong, VIC 3220, Australia. E-mail: joselito.razal@deakin.edu.au, shayan.seyedin@deakin.edu.au
[b] University of Wollongong, Intelligent Polymer Research Institute, Wollongong, NSW 2522, Australia

yarns, or fabrics and their performance are described. These methods include coating a fabric with electrically conducting materials, making conducting elastomeric composite fibers from blend formulations, manipulating nanomaterials into stretchable yarns, and integrating conducting fibers or yarns with fabrics. The sensing mechanisms of various types of textile strain sensors are explained with the emphasis on the resistive and capacitive types because they are more commonly used in textile applications due to their facile fabrication and use.[23] It is shown that the textile sensors enable applications that have direct significant impact in various sectors including health, sports, and entertainment. These applications require sensing various range of movements from small (*i.e.* facial expression, breathing, coughing, phonation, and human pulses) to large (*i.e.* human limbs) extensions. Based on these advances, we will present our critical evaluation of the relevant knowledge gaps and research questions in order to present opportunities that could help shape the future developments of a truly wearable textile sensor.

Classification and performance factors

Imparting the strain sensing functionalities to textiles can occur at various production stages, *i.e.* at the fiber spinning level, during yarn/fabric fabrication, or at the final textile finishing stage.[24] Hence, textile strain sensors can be classified as fiber, yarn, or fabric sensors from a structural perspective. In terms of sensing, textile strain sensors can be categorized as resistive,[9,16,19,22,25–28] capacitive,[29–32] piezoelectric,[33,34] triboelectric,[35] and optical (Fiber Bragg Grating).[36] The resistive and capacitive types are more commonly used in textile strain sensors due to their facile fabrication and use,[23] and hence are the main focus of this review. When considered from applications standpoint, textile strain sensors can be used when mounted onto or stitched to an existing fabric,[5,37–39] integrated with an elastic substrate,[25,40–45] supported by a frame,[16,17] or be self-supporting[19] (without the use of substrate or frame).

Resistive strain sensors are made with one textile electrode layer. Here, the textile serves as a resistor when a voltage is applied and changes its resistance with respect to the magnitude of the applied strain. The resistance change can be due to the changes in the geometry (area (A) and length (L)) of the textile upon stretching. It can also come from the piezoresistive behavior, *i.e.* changes in resistivity (ρ) of the conductive material used in the textile sensor (eqn (1)).

$$R = \frac{\rho L}{A} \tag{1}$$

Capacitive strain sensors are composed of two textile electrode layers separated by an insulating layer called dielectric. When direct current (DC) voltage is applied to the sensor, opposite charges are accumulated on the two electrodes as the current cannot flow between them due to the presence of the insulating dielectric layer. As the result, a capacitance (C) is generated with values that depend on the area (A) of the textile electrodes, the distance between the two electrodes (d), and the relative permittivity (or dielectric constant, ε_r) of the dielectric material (eqn (2), ε_0 is permittivity of free space). Here, the capacitance changes predominantly as the result of geometrical changes (*i.e.* A and d) with stretching and is independent of the resistance of the textile electrodes.

$$C = \frac{\varepsilon_0 \varepsilon_r A}{d} \tag{2}$$

It is crucial that the textile strain sensors are able to withstand large elongation without a significant reduction in mechanical properties. Retaining conductivity under strain during use is also critical for applications of strain sensor textiles.[46] These attributes are very important for many applications and also during the fabrication (*e.g.* weaving, knitting, and braiding) of textiles from sensor fibers or yarns.

The sensing range (*i.e.* strain range at which the sensor reliably work) should cover the full strain range of the desired application.

Shayan Seyedin

Shayan Seyedin is a Research Fellow at the Institute for Frontier Materials, Deakin University. He received his PhD from the University of Wollongong in 2014 for his work on advanced fiber spinning of novel organic electroactive nanocomposites for wearable strain sensing. His research aims to connect science of novel nanoscale materials with advanced fabrication technologies to create next-generation macroscopic structures and devices for wearable energy storage and sensing. He is a recipient of Alfred Deakin Postdoctoral Research Fellowship, Australian Endeavour Research Fellowship, and several other awards.

Joselito M. Razal

Joselito M. Razal is an Associate Professor at Deakin University and a recipient of Australian Research Council Future Fellowship. He was awarded with a PhD in Chemistry in August 2005 by The University of Texas at Dallas for his work on supertough carbon nanotube fibers at The Alan G. MacDiarmid NanoTech Institute. Prior to moving to Deakin University in March 2014, he spent 8 years at the University of Wollongong where he worked on various electromaterials including graphene for energy and bionics applications. His research focus is now on the development of novel nanomaterials and fibers for use in smart wearable devices and intelligent fabrics.

Take walking as an example, the skin on the feet, waist and joints stretches and contracts by as much as 55%.[6] Therefore, textile strain sensors should be fully functional at the sensing range of 0 to 55% strain in order to monitor these relevant body movements. Further, a linear correlation in sensing response (*e.g.* resistance or capacitance) with strain (linearity) is highly desirable,[39] as this will allow facile prediction of the strain applied to the textile from the sensing response.[47] The changes in the sensing response of the textile strain sensor with stretching should be large enough to be easily measured.[39] The amount of the change in sensing response with respect to stretching determines the sensitivity of the textile strain sensor which is expressed by gauge factor (GF). GF is the magnitude of the resistance or capacitance change over applied strain and can be calculated by eqn (3) and (4). In these equations, R_0 and C_0 are the resistance and capacitance of the sensor at the initial (unstretched) state, ΔR and ΔC are the difference between the resistance (R) and capacitance (C) at the stretched state and R_0 or C_0 respectively, and ε is the applied strain ratio. A high GF value means a highly sensitive sensor.

$$\mathrm{GF} = \frac{\Delta R/R_0}{\varepsilon} \quad (3)$$

$$\mathrm{GF} = \frac{\Delta C/C_0}{\varepsilon} \quad (4)$$

The sensing response should also have no (or low) hysteresis. Hysteresis is present when at a specific strain in a cyclic deformation, the sensing signal in loading (stretching) is different than that in unloading (relaxation). The textile strain sensor should also represent high stability when cyclically stretched and relaxed. Cyclic stability refers to the ability of the sensing response to return to its original (unstretched) value after unloading (removal of strain) as well as the ability of the sensor to exhibit similar sensing response at various cycles.[48] As a garment is repeatedly stretched when worn, it is important for wearable applications that the textile strain sensor is stable in more than 100 000 stretching–releasing cycles; this is based on the conservative estimation that the textile sensor is worn about five hours per day for one year and is stretched and relaxed every minute. Also, strain can be applied at various frequencies during wear. To be able to reliably detect fast motions such as kicking, the textile strain sensor needs to be stable at high frequency deformations (>1 Hz). Deviation from the ideal strain sensing behavior are observed from the non-linear response or when there is hysteresis in resistance during cyclic tests.

For wearable applications, it is required that textile strain sensors are lightweight, have the feel of a textile, and are comfortable to wear.[39] In this context, washability also becomes important. Good environmental stability is also necessary for practical applications as textiles are exposed to various environmental (*e.g.* temperature and humidity) conditions during use.[49] From the manufacturing perspective, the fabrication of textile strain sensors should be easily scalable and economically viable.

Fabrication approaches

Textile strain sensors can be fabricated through various approaches such as coating of conductive materials on fiber, yarn, or fabric, using conducting fibrous structures, spinning composite or coaxial fibers, geometrical manipulation of yarns (*e.g.* buckling and coiling), and knitting. These approaches are discussed in detail in the following sections. The properties of various textile strain sensors reported in the literature, are summarized in Table 1.

Coating techniques

Coating fibers, yarns, or fabrics with conductive materials is a facile method of fabricating textile strain sensors. This can be carried out through *in situ* chemical polymerization, vapor-phase polymerization, dip-coating, spray coating, roller coating, and rod coating. Coating approaches can lead to textile strain sensors with high sensitivity and relatively high sensing range. However, high linearity and cycling stability can be challenging to achieve through coating.

On fabrics. In an early work, polypyrrole (PPy)-coated Lycra fabric strain sensor has been achieved by using a chemical polymerization approach.[9] This approach is suitable for producing coated fabrics with conducting polymers such as PPy and poly(3,4-ethylenedioxythiophene):poly(styrenesulfonate) (PEDOT:PSS). A common practice is soaking the fabric in a monomer solution in the presence of a dopant. A separate solution containing an oxidant is added to that mixture to initiate the polymerization process. Alternatively, the fabric can be placed in a solution containing the monomer, the oxidant, and the dopant altogether.[9,50] The optimized polymerization condition for the PPy-coated Lycra fabric achieved sensing up to 60% strain. The resistance of the PPy-coated Lycra fabric decreased with the application of strain with GFs of ~ -3.5 (at 20% strain).

The PPy-coated Tactel/Lycra fabric fabricated by a vapor-phase polymerization (VPP) approach achieved more uniform coating than the *in situ* chemical polymerization approach (Fig. 1a).[49] Here, the textile substrate is soaked in a solution of oxidant and dopant and is then exposed to the vapor of the monomer, resulting in a thin conducting polymer layer on the textile substrate.[49,58] The PPy-coated fabric obtained by the VPP approach[49] sensed by increasing resistance with stretching and showed a higher sensitivity (GF of ~ 80 at 50% strain) and a slightly lower sensing range (50% strain) compared to the fabric coated with the *in situ* polymerization approach.

Conducting polymer composite (CPC) coatings have also been used for fabricating textile strain sensors.[39] A poly[styrene-*b*-(ethylene-*co*-butylene)-*b*-styrene] (SEBS)/carbon black (CB) dispersion in chloroform was prepared and deposited onto a nylon fabric by the aid of a mask and then the electrical connections were established using two stainless steel yarns. While CPC typically leads to a high adhesion of the conducting material to the textile substrate, this approach results in materials with relatively low conductivities due to the presence of non-conducting polymer material in the coating layer. For instance

Table 1 Properties of various textile strain sensors reported in the literature

Sensing mechanism	Fabrication method	Type	Stretchable component	Sensing component	Strain at break (%)	Conductivity (S cm^{-1})	Sensing range	Gauge factor	Cyclic stability	Linearity and hysteresis	Ref.
Resistance	*In situ* chemical polymerization	Fabric	Lycra	PPy	N/A	N/A (resistance ~6 kΩ)	Up to 60%	~−3.5 (at 20% strain) ~−0.7 (at 60% strain)	N/A	Non-linear Low hysteresis	9
Resistance (conductivity)	*In situ* chemical polymerization	Fabric	Nylon/Spandex (95 : 5)	PPy	N/A	~1	Up to 80%	~2.5 (at 80% strain)	~80% in 50 cycles	Non-linear ~19% hysteresis (at 60% strain)	50
Resistance	VPP	Fabric	Tactel/Lycra (83 : 17)	PPy	N/A	N/A	Up to 50%	~80 (at 50% strain)	N/A	N/A N/A	49
Resistance	CPC coating	Fabric	Nylon	SBS/CB	N/A	~5×10^{-4} (CPC layer)	Up to 45%	~80 (at 15–45% strain)	N/A	Non-linear N/A	39
Resistance (conductivity)	Dip-coating	Fabric	Spandex	PEDOT:PSS	N/A	~1.7	Up to 80%	N/A	N/A	Non-linear High hysteresis	51
Resistance	Dip-coating	Fabric	Nylon/PU (97 : 3)	rGO	~270	N/A (resistance ~112 kΩ sq^{-1})	Up to 33%	~18.5 (at 10% strain) ~12.1 (at 10–18% strain)	120 cycles	Non-linear Low hysteresis	18
Resistance	Dip-coating	Fabric	Polyester	Ag	N/A	N/A (resistance ~20 Ω)	6–50%	~5 at 10% strain	1000 cycles (at 10% strain)	Non-linear Low hysteresis	52
Resistance	Dip-coating	Fabric	Cotton	rGO/SWCNT	N/A	N/A	Up to 11.6% bending strain	~5.4 (at 3.3–5.5% bending strain)	100 000 cycles (at 11.6% bending strain)	Non-linear Low hysteresis	53
Resistance	Spray coating	Fabric	PET	PC/CNT	N/A	N/A	Up to 27%	~2.5 (at 0.45–0.6%) ~100 (at 27% strain)	~80% for 400 cycles (at 0.6% strain)	Non-linear High hysteresis	54
Resistance (current)	Spray coating	Fabric	PET	ZnO NW@CNT/ rGO	N/A	N/A	Up to ~6.2% bending strain	~7.6 (at 12.0–6.9 mm bending radius)	200 cycles (at bending rates of 0.2–1 Hz.)	Non-linear N/A	44
Resistance	Vacuum filtration	Fabric	Cotton	rGO	N/A	N/A (resistance ~0.9 kΩ sq^{-1})	5–2.5 cm bending radius	N/A	400 cycles	Non-linear N/A	55
Resistance	Printing	Fabric	Nylon 66	PEDOT:PSS	N/A	~25 (PEDOT:PSS)	Up to 5%	~−5 (at 5% strain)	25 cycles (at 5% strain)	Non-linear High hysteresis	56
Resistance	*In situ* chemical polymerization	Fiber	PU	PANI	N/A	~0.01 (at ~7 wt% PANI)	Up to 1500%	~3 (at 400% strain)	Irreversible signal in 5 cycles (at 50% strain)	Non-linear High hysteresis	57
Resistance	*In situ* chemical polymerization	Fiber	Polyester	PEDOT	N/A	N/A	Up to 20%	~−0.76	1000 cycles (at 10% strain)	Non-linear High hysteresis	37
Resistance	VPP	Fiber	Lycra	PPy	N/A	N/A	Up to 100%	~75 (at 40% strain) ~20 (at 100% strain)	N/A	Non-linear N/A	58
Resistance	CPC roller coating	Yarn	Spandex	PU/CNT	N/A	~0.001 (CPC layer)	Up to 30%	~4.3 (at 10% strain)	Irreversible signal in 15 cycles (at 10% strain)	Non-linear High hysteresis	47
Resistance	CPC/LbL	Yarn	PU	CB/CNC/NR	N/A	N/A	Up to 5%	~38.9 (at 1% strain)	10 000 cycles (at 1% strain)	N/A N/A	45
Resistance	LbL dip-coating	Yarn	RY	GNP	N/A	N/A	Up to 100%	~1800 (at 100% strain)	10 cycles (at ~80% strain)	Non-linear N/A	38
Resistance	LbL dip-coating	Yarn	NCRY	GNP	N/A	N/A	Up to 150%	~1.4 (at 150% strain)	10 cycles (at ~100% strain)	Linear N/A	38
Resistance	LbL dip-coating	Yarn	WY	GNP	N/A	N/A	Up to 50%	~−0.1 (at 50% strain)	10 cycles (at ~40% strain)	Non-linear N/A	38

Table 1 (*continued*)

Sensing mechanism	Fabrication method	Type	Stretchable component	Sensing component	Strain at break (%)	Conductivity (S cm^{-1})	Sensing range	Gauge factor	Cyclic stability	Linearity and hysteresis	Ref.
Resistance	Dip-coating	Yarn	Cotton/PU core-spun yarn	SWCNT	N/A	N/A	Up to ~300%	~0.65 (at 25–240% strain)	300 000 cycles (at 40% strain)	High linearity (at 25–240% strain) N/A	21
Resistance	Dip-coating	Yarn	PDCY (PU/PE)	rGO	676	1.4×10^{-3} (6 coating cycles)	Up to 200%	~10 (at 1% strain) ~3.7 (at 50% strain)	10 000 cycles (at 30% and 50% strains)	Non-linear High hysteresis	25
Resistance	Electrospinning/ dip-coating	Yarn	Rubber/PU core–shell thread	P(VDF–TrFE)/ AgNW	N/A	N/A (resistance 5 Ω cm^{-1}, 7 coating cycles)	Up to 50%	~5.3 (at 25% strain)	~90% in 10 000 cycles (at 5% strain)	High linearity (at 10–50% strain) Low hysteresis	59
Resistance	Roll-to-roll coating	Yarn	Polyolefin	AgNW	~550	N/A (resistance ~10 Ω)	Up to 64%	Up to ~13 920 (at ~55% strain)	4500 cycles (at 10% strain)	Non-linear N/A	60
Resistance	Rod coating	Fiber	Spandex	Graphite flakes	~33	N/A	Up to 30%	14 (at ~30% strain)	N/A	Non-linear N/A	61
Resistance	Rod coating	Fiber	PP	Graphite flakes	~20	N/A	Up to ~18%	14.2 (at ~18% strain)	N/A	Non-linear N/A	61
Resistance	Rod coating	Fiber	Silk	Graphite flakes	~17	N/A	Up to ~15%	14.5 (at ~15% strain)	3000 cycles (at 10% strain)	Non-linear Low hysteresis (at 5% strain)	61
Resistance	Hydrothermal growth	Fiber	PU	ZnO NW	N/A	N/A	1.8–150%	~15.2 (at <10% strain) ~4.1 (at 10–150% strain)	10 000 cycles (at 8.7–23.2% strain)	High linearity (at 10–150% strain) High hysteresis	62
Resistance	Non-elastic conducting fiber	Fiber	None	Carbon fiber	N/A	~455	Up to 1.2%	~2 (at 1% strain)	N/A	High linearity (at 1% strain) N/A	63
Resistance	CVD	Yarn	None	CNT	N/A	N/A	Up to 1%	~0.5 (at 1% strain)	N/A	High linearity (at 1% strain) N/A	48
Resistance	CVD	Yarn	None	CNT	~3.6	N/A	Up to ~3.6%	~12 (at ~1.2% strain)	10 cycles (at 1% strain)	High linearity (at 1% strain) Low hysteresis (at 1% strain)	64
Resistance	Dry-spinning	Yarn	Ecoflex	CNT	N/A	~0.001	Up to 960%	0.54 (at 0–400% strain) ~64 (at 400–960% strain)	~93% in 10 000 cycles	Non-linear N/A	43
Resistance	CVD (Cu mesh as template)	Fabric	PDMS	Graphene	N/A	N/A (resistance ~200–2500 Ω sq^{-1})	Up to 12%	~1250 (at 2% strain) ~4600 (at 5% strain)	5 cycles (at 2 and 5% strains)	Non-linear High hysteresis	40
Resistance	CVD (Ni fabric as template)	Fabric	PDMS	Graphene	N/A	~2.7	Up to 3%	223 (at 3% strain)	1000 cycles (at 3% strain)	High linearity (at 3% strain) Low hysteresis (at 3% strain)	41
Resistance	Carbonization	Fabric	Ecoflex	Carbonized silk fabric	N/A	N/A (resistance 140 Ω sq^{-1})	Up to 520%	~9.6 (at 0–250% strain) ~37.5 (at 250–500% strain)	~80% after 10 000 cycles (at 300% strain)	High linearity (at 0–250% or 250–500% strains) High hysteresis	42
Resistance	Carbonization	Fabric	Ecoflex	Carbonized cotton fabric	N/A	N/A (resistance 80 Ω sq^{-1})	Up to ~140%	~25 (at 0–80% strain) ~64 (at 80–140% strain)	2000 cycles (at 50% strain)	Non-linear High hysteresis	26

Table 1 (*continued*)

Sensing mechanism	Fabrication method	Type	Stretchable component	Sensing component	Strain at break (%)	Conductivity (S cm^{-1})	Sensing range	Gauge factor	Cyclic stability	Linearity and hysteresis	Ref.
Resistance	Dip-coating/ pyrolyzing	Fabric	Rubber latex	rGO/pyrolyzed cotton	~950	N/A	Up to 57%	~416 (at 0–40% strain) ~3667 (at 48–57% strain)	1000 cycles (at 7.5% strain)	High linearity (at 40% strain) N/A	65
Resistance	Melt-spinning composite fiber	Fiber	SEBS	CB	N/A	N/A (resistance 700 Ω cm^{-1} at 50 wt% CB)	20–80%	~20 (at 80% strain)	~2.5% resistance increase in ~3800 cycles	Non-linear Hysteresis ±5.5% strain	5
Resistance	Melt-spinning composite fiber	Fiber	PU	MWCNT	N/A	~0.03 (at 3 wt% MWCNT)	Up to 10%	N/A	15 cycles (at 10% strain)	Non-linear High hysteresis	66
Resistance	Melt-spinning composite fiber	Fiber	PC	MWCNT	~8.3 (6 wt% MWCNT, draw ratio 4.83)	~0.03 (at 6 wt% MWCNT, draw ratio 4.83)	Up to ~6%	~16 (at 1.8% strain, 3.5 wt% MWCNT, draw ratio 8.1)	N/A	Non-linear N/A	67
Resistance	Wet-spinning composite fiber	Yarn	PANI	NR	580 (at 5 wt% PANI)	1×10^{-3} (at 5 wt% PANI) 1.7×10^{-3} (at 10 wt% PANI)	N/A	N/A	N/A	N/A N/A	68
Resistance	Wet-spinning composite fiber	Fiber	SIBS	P3HT	~975 (at ~14 wt% P3HT)	~0.38 (at ~14 wt% P3HT)	12.25% after ~800–900% pre-strain	~−1.6 (at 12.25% strain)	20 cycles	Non-linear High hysteresis	46
Resistance	Wet-spinning composite fiber	Fiber	PU	PEDOT:PSS	~345 (at ~13 wt% PEDOT:PSS)	~9.4 (at ~13 wt% PEDOT:PSS) ~25 (at ~25 wt% PEDOT:PSS)	Up to ~260%	$\sim 10^4$ (at 200% strain)	10 cycles (at 100% strain)	Non-linear High hysteresis	27
Resistance	Wet-spinning composite fiber	Fiber	PU	rGO	~318 (at ~2.9 wt% GO)	~0.002 (at 6.9 wt% GO)	Up to 70%	N/A	10 cycles (at 40% strain)	Non-linear High hysteresis	69
Resistance	Wet-spinning composite fiber	Fiber	PU	CB	~296 (at 16.7 wt% CB)	~0.014 (at 16.7 wt% CB)	Up to ~50%	N/A	10 cycles (at 40% strain)	Non-linear High hysteresis	70
Resistance	Wet-spinning composite fiber	Fiber	PU	SWCNT	~119 (at ~4.8 wt% SWCNT)	~0.007 (at ~4.8 wt% SWCNT)	Up to ~60%	N/A	10 cycles (at 30% strain)	Non-linear High hysteresis	70
Resistance	Wet-spinning composite fiber	Fiber	PU	CCG	~56 (at ~6 wt% CCG)	~0.004 (at ~12.5 wt% CCG)	Up to ~40%	N/A	10 cycles (at 20% strain)	Non-linear High hysteresis	70
Resistance	Wet-spinning composite fiber	Fiber	SBS	AgNW/AgNP	~900 (at 0.6 wt% AgNW, 75 wt% AgNP)	~2450 (at 1.7 wt% AgNW, 75 wt% AgNP)	Up to ~100%	~15 (at 100% strain)	~100% resistance increase in 1000 cycles (at 10% strain)	Non-linear High hysteresis	71
Resistance	Wet-spinning composite fiber	Fiber	PU	AgNW	~348 (at 38 wt% AgNW)	~1656 (at 38 wt% AgNW) ~14 205 (at 38 wt% AgNW)	Up to 20%	~1.5 (at 20% strain)	~13% resistance increase in 50 cycles (at 20% strain)	Non-linear High hysteresis	72
Resistance (conductivity)	Wet-spinning composite fiber	Fiber	SIBS	SWCNT	~828 (at ~3.8 wt% SWCNT)	~0.08 (at 3.8 wt% SWCNT)	Up to 30%	N/A	10 cycles (at 10–30% strain)	Non-linear High hysteresis	73
Resistance	Wrapping/ buckling	Fiber	Rubber	CNT	N/A	N/A	Up to 600%	~0.5 (at 0–200% strain) ~0.14 (at 200–600% strain)	5000 cycles (at 100–600% strain)	High linearity (at 200% strain) Low hysteresis (at 600% strain)	22
Resistance	Buckling/ twisting	Fiber	PU	AgNW	417	1.4×10^4	~400% (up to 10 kPa pressure)	N/A (0.12 kPa^{-1} at 2 kPa, 0.012 rad^{-1} at $2\pi/3$)	4000 cycles (at 100% strain)	Non-linear N/A	74

Table 1 (*continued*)

Sensing mechanism	Fabrication method	Type	Stretchable component	Sensing component	Strain at break (%)	Conductivity (S cm^{-1})	Sensing range	Gauge factor	Cyclic stability	Linearity and hysteresis	Ref.
Resistance	Full-helical	Yarn	None	SWCNT	~285	~440	Up to 20%	~0.1 (at 20% strain)	~90% in 1000 cycles	Non-linear High hysteresis	75
Resistance	Partial-helical	Yarn	None	SWCNT	N/A	N/A (resistance ~11 Ω)	Up to 25%	0.14 (at 0–5% strain) 0.03 (at 5–25% strain)	~1.7% resistance decrease in 1000 cycles (at 25% strain)	High linearity (at 0–5% or 5–25% strain) High hysteresis	28
Resistance	Overtwisting	Fiber	None	CNT	985	N/A	Up to 500%	0.13 (at 500% strain)	600 cycles (at 500% strain)	Non-linear High hysteresis	76
Resistance	LM injection	Fiber	SEBS	EGaIn	800–1000	~3.3 × 10^4	Up to ~600%	N/A	N/A	Non-linear N/A	77
Resistance	LM injection	Fiber	PDMS	EGaInSn	N/A	~2.9 × 10^3	Up to 140%	3.4 (at 140% strain)	3500 cycles (at 70% strain)	High linearity (at 140% strain) Low hysteresis (at 140% strain)	78
Resistance	CVD/coating	Fiber	PVA	Graphene	16 (at 10 wt% PVA)	96 (at 10 wt% PVA)	Up to 6.3%	~5.0 (at 1–6.3% strain)	200 cycles (at 6% strain)	Non-linear N/A	79
Resistance	Wet-spinning coaxial fiber	Fiber	Silicone rubber	MWCNT/silicone rubber	~800	~0.02 (at 3.5 wt% MWCNT)	>300%	~0.68 (at 50–100% strain) 1378 (at 300–330% strain)	10 000 cycles (at 100% strain)	Non-linear Low hysteresis (at 150% strain)	80
Resistance	Wet-spinning coaxial fiber	Fiber	Polystyrene-*b*-polyisoprene-*b*-polystyrene	SWCNT	N/A	N/A	Up to 250%	~48 (at 5% strain) ~425 (at 20–100% strain)	~10% resistance increase in 3250 cycles (at 20–100%)	High linearity (at 0–5% or 20–100% strain) Low hysteresis (at 100% strain)	81
Resistance	Fill and seal	Fiber	PDMS	Ionic liquid	230	N/A	Up to 100%	~2.8 (straight channel) <0.5 (helical channel)	10 000 cycles (at 40% strain)	High linearity (at 100% strain) Low hysteresis (at 100% strain)	82
Resistance	Knitting	Fabric	Lycra yarn	Silver-coated nylon	~160–440	N/A (resistance 125–170 Ω)	Up to 40%	0.08–2.5 (at 40% strain)	N/A	Non-linear High hysteresis	23
Resistance	Knitting	Fabric	Spandex yarn	CNT	900 (1 Spandex yarn)	70.9 (1 Spandex yarn)	Up to 100%	Up to ~0.4 (at 100% strain for 12 Spandex yarns)	97.7% in 1000 cycles (at 100% strain)	Non-linear Low hysteresis (at 100% strain)	17
Resistance	Knitting	Fabric	Spandex yarn in some structures	PU/PEDOT:PSS monofilament	~345	~9.4	Up to ~180% (four-ply PU/PEDOT:PSS fiber)	~−1 (at 160% strain for four-ply PU/PEDOT:PSS fiber)	500 cycles (at 100% strain) after initial resistance decrease	Non-linear High hysteresis	16
Resistance	Knitting	Fabric	Polyester yarn in some structures	PU/PEDOT:PSS multifilament	~415	~5.4	Up to 200%	~−0.7 (at 50% strain for plain-knit fabric)	500 cycles (at 100% strain) after initial resistance decrease	Non-linear High hysteresis	19
Capacitance	Wrapping/buckling	Fiber	SEBS rubber	CNT	N/A	3.6 (at 870% strain)	Up to 950%	0.91 (at 950% strain)	500 cycles (at 950% strain)	High linearity (at 950% strain) Low hysteresis (at 950% strain)	29
Capacitance	Wrapping/buckling	Fiber	SEBS rubber	CNT	N/A	~0.03 (~1.95 at 800% strain)	Up to 200%	~0.6 (at 200% strain)	5000 cycles (at 40% strain)	High linearity (at 200% strain) Low hysteresis (at 200% strain)	83

Table 1 (*continued*)

Sensing mechanism	Fabrication method	Type	Stretchable component	Sensing component	Strain at break (%)	Conductivity (S cm^{-1})	Sensing range	Gauge factor	Cyclic stability	Linearity and hysteresis	Ref.
Capacitance	Wrapping/ buckling/ twisting	Fiber	Ecoflex	CNT	N/A	N/A (resistance 179 Ω cm^{-1})	Up to 200% (150° bending, 1700 rad m^{-1} twisting)	~0.6 (at 200% strain)	200 cycles (at 200% strain)	High linearity (at 200% strain) Low hysteresis (at 200% strain)	30
Capacitance	LM injection	Yarn	Hytrel	EGaIn	N/A	N/A	Up to ~100%	~0.82 (at ~100 strain)	N/A	High linearity (at 100% strain) N/A	32
Capacitance	Multicore-shell printing	Fiber	Silicone (Dragonskin 10)	Ionic conductor (glycerol mixture)	700–800	0.005–0.03	Up to 250%	0.35 (at 100% strain)	N/A	Non-linear Low hysteresis (at 150% strain)	84
Capacitance	Laser cutting	Fabric	Silicone elastomer	Silver-plated knitted fabric	N/A	N/A	Up to 100%	1.23 (at 100% strain)	~78% after 1000 cycles (at 100% strain)	High linearity (at 100% strain) Low hysteresis (at 100% strain)	31

in the SEBS/CB-coated fabric, a maximum electrical conductivity of ~0.05 S cm^{-1} was obtained for a CB concentration of ~28 vol%. This coated fabric showed strain sensing behavior until the breaking strain (~45% strain) with a GF of ~80 (15–45% strain). The resistance response of the coated fabric showed a non-linear relationship with strain when the fabric was stretched more than 15%.

Textile strain sensors can be achieved by dip-coating textiles in a solution or dispersion of a conductive material. For example, after 5 min of soaking, a Spandex fabric in aqueous PEDOT:PSS dispersion resulted in an electrically conductive (~0.06 S cm^{-1}) stretchable fabric (Fig. 1b).[51] Multiple soaking and drying was shown to increase the conductivity of the fabric, reaching a maximum conductivity of ~1.7 S cm^{-1} after 10 dipping cycles. Further increase in dipping cycles only resulted in the delamination of coating from the Spandex substrate. The conductivity was also found to depend on the weaving pattern, porosity, and hydrophilicity of the fabric substrate.[51] While the PEDOT:PSS-coated Spandex fabric remained highly stretchable (~200%), its conductivity decreased ~70% after 5 days of storage in air. The conductivity of the fabric increased with stretching with some hysteresis in the resistance response; ~13% and ~65% conductivity losses were observed after relaxation from 20% and 100% strains, respectively.

Silver-coated (Ag-coated) fabric strain sensors were also fabricated by dip-coating plasma-cleaned knitted polyester fabrics in a reactive silver ink for 5 min and then annealing at 90 °C for 15 min (Fig. 1c).[52] Although the resistance response of the Ag-coated fabric decreased with stretching below 6% strain, it increased when the fabric was stretched to 50%. The Ag-coated fabric sensor showed high stability under 1000 stretching–releasing cycles at 10% strain with an estimated GF of ~−5. While the Ag-coated fabric showed a small resistance change after 30 min washing with water, the resistance increased by ~5 times after washing the fabric for 70 min due to the exfoliation of the Ag coating, which indicated low washability. Recently, a waterproof rGO/single wall carbon nanotube (SWCNT) coated fabric strain and pressure sensor was achieved by a sequential dip coating of a cotton fabric in GO and SWCNT dispersions (Fig. 1d).[53] The resulting fabric could sense bending strains of up to ~11.6% (Fig. 1e–g). The fabric showed a GF of ~5.4 (lower than rGO coated cotton fabric, GF ~ 6.1) at the bending region of 3.3–5.5%, which decreased to ~1 at bending strain of 9.3–11.6% (Fig. 1h). While the resistance of the rGO coated fabric decreased ~9% after 10^5 cycles at 11.6% strain, increasing the SWCNT content significantly enhanced the sensing stability. The rGO/SWCNT coated fabric displayed unchanged sensing response after 10 times of washing.

Spray coating can also be used to deposit layers of conducting materials on fabrics to achieve fabric strain sensors. The thickness of the coating could easily be controlled by the number of spraying layers.[54] For instance, by spray coating a fabric with piezoresistive ZnO nanowires (NW), a textile strain sensor was produced (Fig. 1i).[44] This fabric sensor was prepared by first spray coating chemically modified CNT and chemically exfoliated rGO suspensions on oxygen plasma treated

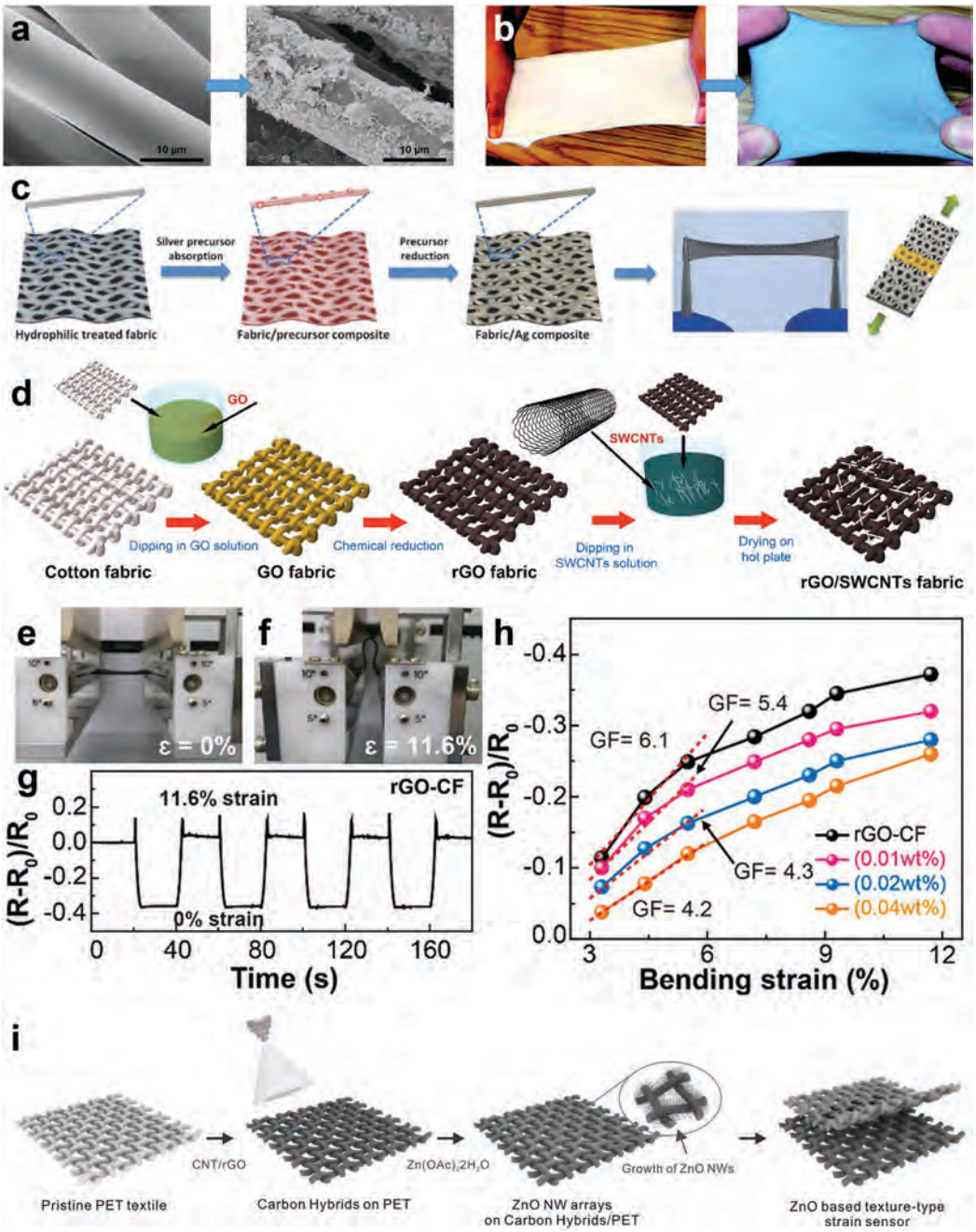

Fig. 1 (a) SEM images a plain-knitted fabric before and after coating with PPy using an *in situ* chemical polymerization approach. Adapted with permission.[49] Copyright 2010 Elsevier Ltd. (b) Photos of a Spandex fabric before and after soaking with PEDOT:PSS. Adapted with permission.[51] Copyright 2010 American Chemical Society. (c) Schematic illustration of the fabrication process of silver-coated fabric strain sensor. Adapted with permission.[52] Copyright 2017 John Wiley & Sons, Inc. (d) Schematic illustration of the fabrication process, (e and f) testing setup, and (g and h) strain sensing properties of rGO/SWCNT coated fabric strain sensor. Adapted with permission.[53] Copyright 2010 American Chemical Society. (i) Schematic illustration of the fabrication of ZnO coated fabric strain sensor. Adapted with permission.[44] Copyright 2017 John Wiley & Sons, Inc.

poly(ethylene terephthalate) (PET) fabric. After drying, well-aligned ZnO NW were grown on the CNT/rGO coated fabric using a hydrothermal method at 90 °C and the structure was embedded within a polydimethylsiloxane (PDMS) layer to protect the sensor assembly from mechanical deformations. The ZnO NW@CNT/rGO coated fabric could sense low bending strains of up to ~6.2% with a GF of ~7.6 that is higher than the film counterpart (GF ~ 4.57). The sensing response was found to be stable for 200 cycles at bending rates for up to 1 Hz.

Textile strain sensors were also fabricated *via* vacuum filtration of GO aqueous dispersion on a cotton fabric (3 × 1 cm^2); GO reduction was carried out by hot pressing at 180 °C.[55] Sensing in stretching (increased resistance by ~10 times) and in compression (decreased resistance by ~2.3 times) was found

stable for 400 cycles. The washability test revealed a ~33% increase in resistance after 10 washing cycles with detergent at 60 °C for 30 min.

On fibers or on yarns. Fiber and yarn strain sensors are also made by coating with conductive materials. For example, polyaniline (PANI)-coated PU fibers prepared by *in situ* polymerization showed a maximum conductivity of ~0.01 S cm^{-1} at PANI content of ~7 wt%.[57] These fibers could detect strains of up to ~1500% and had a GF of ~3 at 400% strain. However, the strain sensing became irreversible with significant hysteresis when stretched to 50% for 5 cycles. Also, the conductivity decreased by 1000 times after washing with water for 5 min. A fiber strain sensor was also fabricated by coating PEDOT on polyester fiber using the *in situ* polymerization approach and then coating with poly(methyl methacrylate) PMMA for encapsulation of conductive layer (Fig. 2a).[37] The fiber sewn onto a fabric could sense up to 20% strain and showed a negative GF of ~−0.76 (resistance decreased with stretching). A considerable increase in the resistance response was observed when the PEDOT-coated fiber sensor was repeatedly stretched

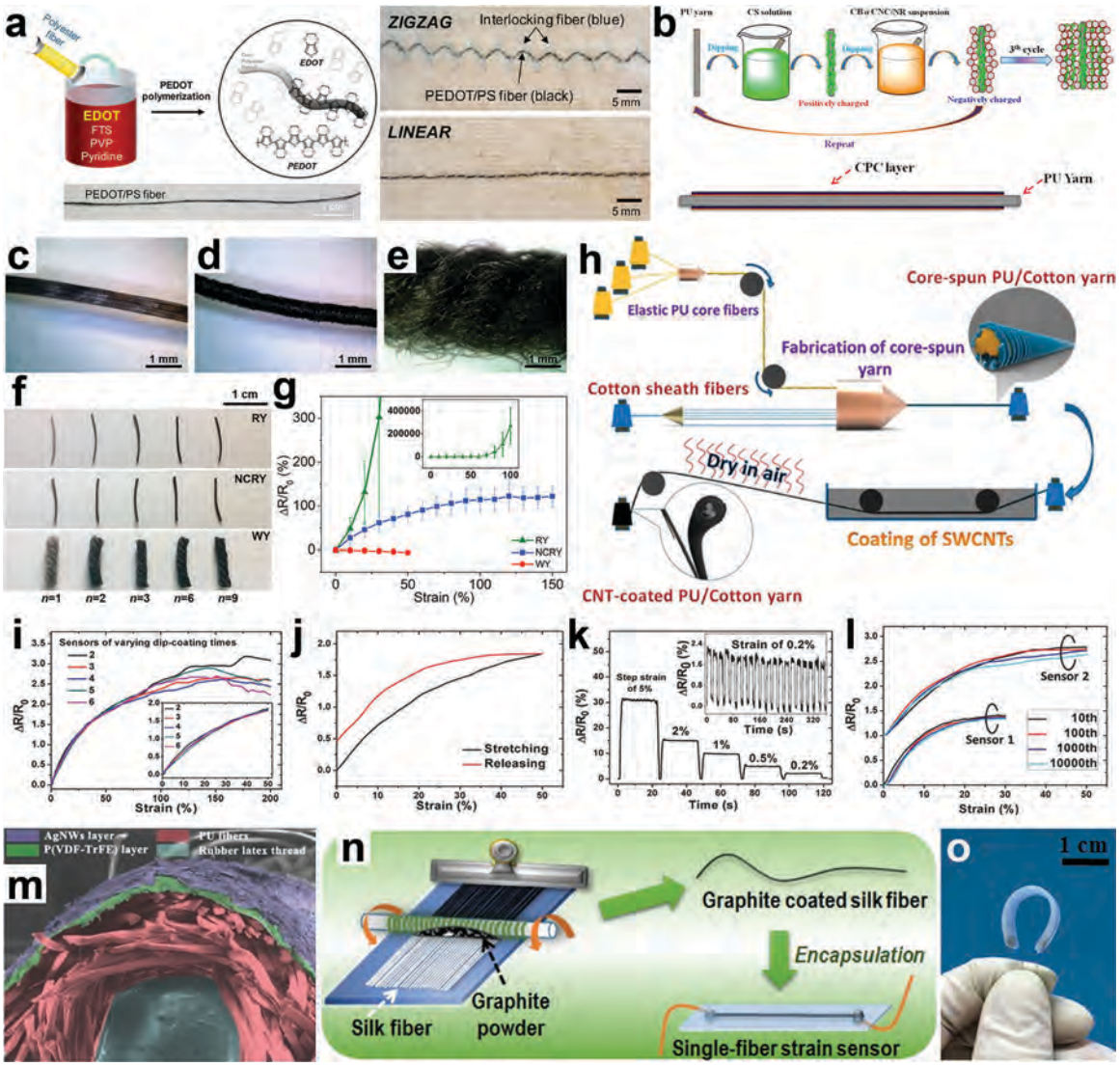

Fig. 2 (a) Schematic illustration of *in situ* polymerization of PEDOT on a PS fiber and photos of the coated fiber after being sewn on a fabric. Adapted with permission.[37] Copyright 2017 American Chemical Society. (b) Schematic illustrations for the preparation of the CPC coated PU yarn using LbL assembly. Adapted with permission.[45] Copyright 2016 American Chemical Society. Photos of (c) RY, (d) NCRY, (e) WY yarn strain sensors obtained LbL coating with PVA and GNP, and (f) at various LbL cycles. (g) Strain sensing properties of the RY, NCRY, and WY yarns. Adapted with permission.[38] Copyright 2015 American Chemical Society. (h) Schematic illustration of the fabrication process of the SWCNT-coated core-spun yarn strain sensor. Adapted with permission.[21] Copyright 2016 American Chemical Society. (i–l) Strain sensing performance of rGO–PDCY yarn sensor: (i) relative resistance change with strain, (j) relative resistance change with strain for one stretching and releasing cycle, (k) relative resistance at various strains, and (l) stretching–releasing cyclic tests at 30% strain on sensor 1 and at 50% on sensor 2 (baseline upshifted). Adapted with permission.[25] Copyright 2015 John Wiley & Sons, Inc. (m) SEM image of the cross section of AgNW coated core-spun yarn. Adapted with permission.[59] Copyright 2016 John Wiley & Sons, Inc. (n) Schematic illustration of Meyer rod coating process and (o) photo of graphite-coated silk fiber strain sensor. Adapted with permission.[61] Copyright 2016 American Chemical Society.

and released for 1000 cycles at 20% strain, indicating its low stability.

CPC coated yarn strain sensors were also produced using a layer-by-layer (LbL) method by sequentially dipping a PU yarn into a negatively charged CB/cellulose nanocrystals (CNC)/natural rubber (NR) suspension and then into a positively charged chitosan solution (Fig. 2b).[45] The strain sensor was achieved by embedding the CPC coated PU yarn into a PDMS matrix. While this CPC-coated PU yarn based sensor could detect strains as low as 0.1%, it was not reliable for sensing strains larger than 5%. The sensor with 50 coating layers showed a GF of ~38.9 at 1% strain that was stable for 10 000 stretching–releasing cycles at 1% strain. The CPC coated PU yarn showed good washability with ~23% and ~37% resistance increases after 24 h of washing with detergent and 5 h of washing with boiling water.

Yarn strain sensors were also fabricated by LbL dip-coating of polyvinyl alcohol (PVA) and graphene nanoplatelets (GNP) on various yarns *e.g.* rubber (RY), nylon covered rubber (NCRY), and wool yarns (WY) with thicknesses ranging from ~0.33 mm to ~3 mm (Fig. 2c–f).[38] The yarn sensors were coated with PDMS to avoid delamination of the GNP coating when undergoing high strains. These yarn sensors possessed different sensing ranges (50% to 150%) and sensitivities (Fig. 2g) with GFs of up to ~1800 (RY), 1.4 (NCRY), and −0.1 (WY). These yarn sensors also showed high stability and fast response when tested under 10 stretching–releasing cycles at strains of ~80% (RY), ~100% (NCRY), and ~40% (WY). While these yarn textile sensors showed high sensing performance, they used an additional PDMS coating layer that can change the feel of the textile. A yarn strain sensor that did not require further coating with an elastic layer, was fabricated by first producing a core-spun yarn through winding cotton yarn around an elastic PU filament and then dip-coating with SWCNT, (Fig. 2h).[21] The SWCNT-coated core-spun yarn strain sensor (achieved by 12 dip-coating cycles) could sense up to ~300% strain, albeit with a relatively low GFs of ~0.65 (between 25% and 240% strain). The sensor's response was stable for up to 300 000 cycles at 40% strain. It could also operate at 15 Hz of 10% stretching vibrations. Such high cycling stability and operation at high frequencies are desirable for wearable applications. In another study, a double-covered yarn (PDCY) composed of a PU fiber core and helically wound PE fibers was dip coated in a GO dispersion and then reduced using HI to achieve a yarn strain sensor.[25] The rGO–PDCY sensor s a conductivity of 1.4×10^{-3} S cm^{-1} after 6 dip-coating cycles. When examined after 2 dip-coating cycles, the mechanical properties was found similar to the original uncoated yarn (elongation at break ~676% and tensile strength ~29.1 MPa). The resistance of the rGO–PDCY sensor increased monotonically with strain before plateauing at 200% (Fig. 2i and j). The rGO–PDCY sensor resulted in high sensitivity with an average GF of ~10 and ~3.7 at 1% and 50% strains, respectively. The sensing response was stable for 10 000 stretching–releasing cycles for up to 50% strain (Fig. 2k and l). Furthermore, the rGO–PDCY sensor mounted on a PDMS slab was also capable of sensing of up to 90° of bending deformations as well as both clockwise (up to −280 rad m^{-1}) and counter clockwise (up to 800 rad m^{-1}) torsional deformations.

Yarn strain sensors were also achieved by first coating core-spun elastic threads with poly(vinylidene difluoride–trifluoroethylen) known as P(VDF–TrFE) nanofiber mat using electrospinning and then dip-coating them in AgNW dispersion while in the stretched state.[59] This yarn sensor (Fig. 2m) showed a linear sensing response for up to 50% strain and retained ~90% of its original sensitivity after 10 000 stretching–releasing cycles at 5% strain. The P(VDF–TrFE)-based sensor showed a GF of ~5.3 at 25% strain, which decreased to ~0.7 at 50% strain. This sensor could also sense bending (up to 130°) and torsional (up to 3000 rad m^{-1}) deformations.

A rod coating approach was also used to achieve fiber strain sensors from various fibers, *e.g.* Spandex, polypropylene (PP), silk fibers, and human hair (Fig. 2n).[61] These fibers were aligned on a flat plate and coated for 10 times with dry graphite flakes by rolling a Meyer rod. Fiber strain sensors were then achieved by encapsulating the graphite-coated fibers within silicone rubber (Fig. 2o). The respective GF and sensing range of the sensors varied depending on the fiber used and were ~14.0 and ~30% for Spandex, ~14.2 and ~18% for PP, ~14.5 and ~15% for silk, and ~71.1 and ~10% for human hair. The silk fiber sensor showed low drift, low hysteresis, and excellent sensing stability during 3000 stretching–releasing cycles at 10% strain. Interestingly, the sensing response of the graphite-coated silk fiber was independent of the strain rate when tested at frequencies ranging from 0.25 to 6 Hz.

Non-elastic conducting fibrous structures

Neat fibers, yarns, or fabrics of conducting materials can exhibit strain sensing properties despite their generally low stretchability. For example, individual carbon fibers with conductivity of up to ~500 S cm^{-1} were shown to sense low strains of up to 1.2% with a GF of ~2.3.[63] A CNT yarn strain sensor was fabricated by spinning of CNT arrays drawn from chemical vapor deposition (CVD)-grown CNT forest (Fig. 3a).[48] The pure CNT yarn showed a limited sensing range of 1% strain and a GF of ~0.5. CNT yarn sensors were also made by direct spinning (without twisting) from CVD synthesis zone of a furnace.[64,85] The sensing range of ~3.6% strain and GF of ~12 (at ~1.2% strain) were achieved. The cyclic test at 1% strain revealed good stability for 10 cycles with a low hysteresis. The GF of the CNT fiber decreased proportionally to the amount of adsorbed water (from ~6.3 at 3% RH to ~2.5 at 100% RH), although the characteristic shape of resistance *vs.* stress curves (including the width of hysteresis loops) and the stress–strain behavior of the yarn remained unchanged with varying RH. By directly attaching highly aligned dry-spun CNT yarns to an elastic substrate (Ecoflex), further improvements in sensing range, sensitivity, and stability of CNT yarn strain sensors were achieved.[43] The CNT yarn on the Ecoflex substrate could be stretched to ~900% while the pure dry-spun CNT yarns failed when the strain was more than 8% (Fig. 3b). Despite its lower conductivity (~0.001 S cm^{-1}) than the pure CNT yarn (~0.1 S cm^{-1}), it could sense strains as large as 440% with GFs of ~0.56 between 0 to 200% strain and ~47 between 200 to 440% strain. By pre-stretching the elastic substrate to 100% before attaching the CNT yarn, the sensing range was

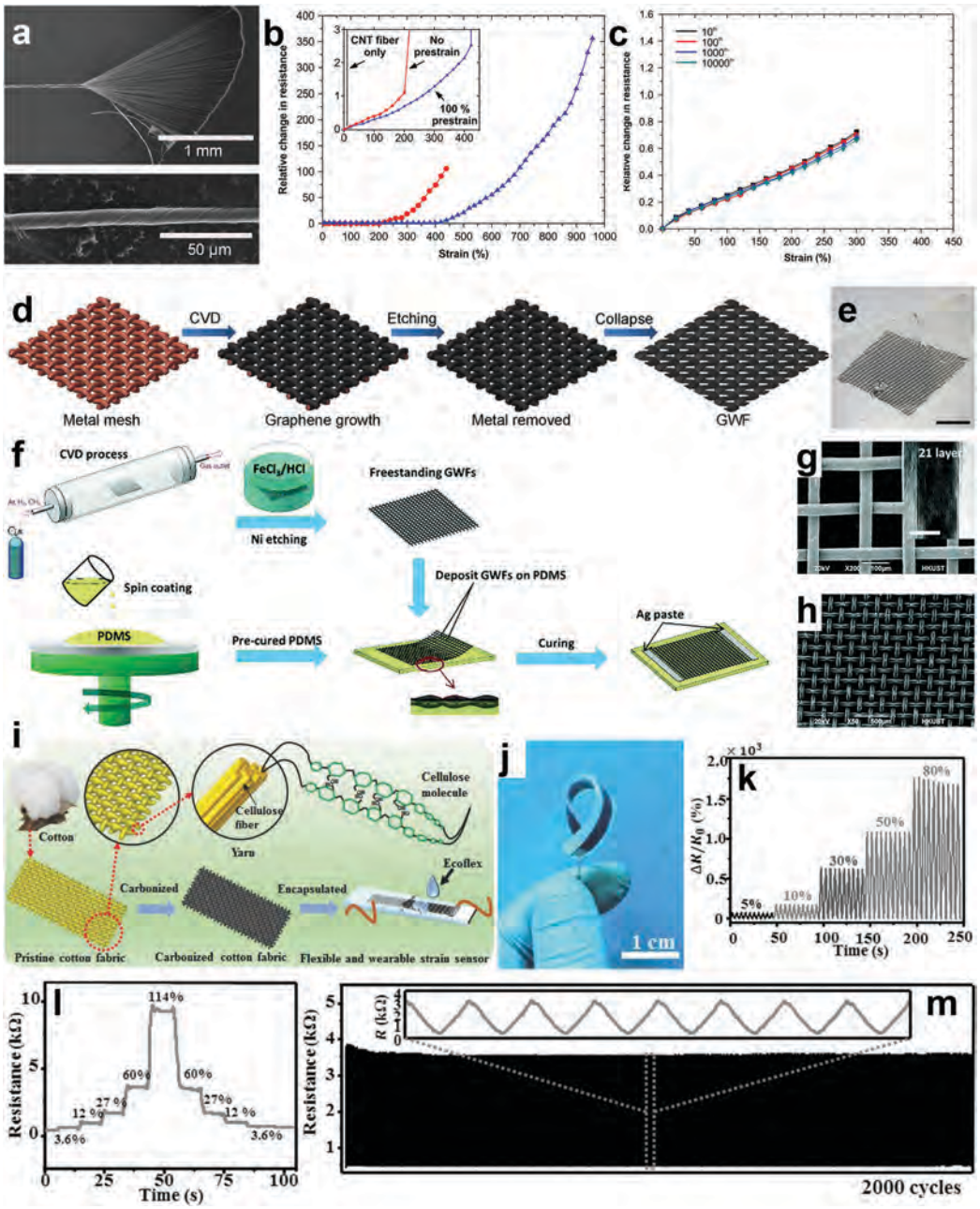

Fig. 3 (a) CNT yarn spinning process to fabricate yarn strain sensor. Adapted with permission.[48] Copyright 2010 IOP Publishing Ltd. (b) Relative change in resistance *vs.* strain for CNT yarn strain sensors before and after mounting on an Ecoflex substrate and pre-stretching and (c) stability of the CNT yarn strain sensors during cyclic stretching–releasing test. Adapted with permission.[43] Copyright 2015 American Chemical Society. (d) Schematic illustration of steps in the preparation of graphene woven fabric (GWF) and (e) photo of GWF deposited on a glass substrate. Adapted with permission.[40] Copyright 2012 Nature Publishing Group. (f) Schematic flowchart of the fabrication process of GWF strain sensor on a PDMS substrate, (g) SEM and TEM images of GWF, and (h) SEM image if GWF strain sensor on PDMS. Adapted with permission.[41] Copyright 2017 Royal Society of Chemistry. (i) Schematic illustration of the fabrication process, (j) photo, and (k–m) strain sensing performance of carbonized cotton fabric strain sensor: (k) relative resistance change under various cyclic strains, (l) resistance response of the sensor when held at different strains, and (m) stability of the sensor under cyclic stretching–releasing. Adapted with permission.[26] Copyright 2016 John Wiley & Sons, Inc.

further extended to an extremely high strain of 960% with GFs of 0.54 between 0 to 400% strain and ~64 between 400 to 960% strain. When the CNT yarn sensor on the pre-stretched substrate was subjected to cyclic deformations at 300% strain, the sensor showed a stable GF of ~0.26 after 10 cycles, which decreased only by ~7% (GF ~ 0.24) after 10 000 cycles (Fig. 3c).

Graphene woven fabric (GWF) strain sensor was fabricated by growing graphene on a copper mesh using CVD method and removing the copper support followed by deposition onto PDMS substrate (Fig. 3d and e).[40] The GWF could sense low strains of 12% with a large GF of ~4600 at 5% strain. The stability of the GWF sensor was shown for 5 stretching–releasing cycles at 2 and

5% strains and the resistance response exhibited noticeable hysteresis. Other GWF strain sensors were achieved using a CVD method with Ni woven fabric as template following the deposition onto a PDMS thin film (Fig. 3f–h).[41] It was observed that the conductivity and sensitivity (GF) of the fabric increased with graphene layers and reached $\sim$2.7 S cm^{-1} and $\sim$223 (at the maximum strain of 3%), respectively. The fabric showed excellent stability when tested under 1000 stretching–releasing cycles at 3% strain. It was found that the sensitivity of the GWF sensor was largely dependent on the testing direction. This is an important observation that should be considered when testing textile strain sensors.

Fabric strain sensors were also fabricated by simply carbonizing silk fabric using a thermal treatment and then encapsulating the fabric within an elastic Ecoflex substrate.[42] This sensor could sense strains as large as 500% and showed GFs of $\sim$9.6 at 0 to 250% strain and $\sim$37.5 at 250 to 500% strain. It also exhibited fast response ($\sim$70 ms), low creep, and high cyclic stretching–releasing stability with $\sim$80% of the sensitivity remaining after 10 000 cycles at 300% strain. Similarly produced carbonized cotton fabric strain sensors (Fig. 3i and j) showed improved sensitivity (GFs of $\sim$25 at 0 to 80% strain and $\sim$64 at 80 to 140% strain) albeit at a lower sensing range of $\sim$140% strain (Fig. 3k and l).[26] This fabric strain sensor could detect strains as low as 0.02% and exhibited almost no frequency dependence sensing response (at 0.05 to 0.25 Hz), negligible drift when held at various strains from 3.6% to 114%, and high cyclic stability for 2000 cycles at 50% strain (Fig. 3m). In another work, a fabric strain sensor was achieved by encapsulation with natural rubber latex the pyrolyzed GO dip-coated cotton bandage.[65] While the sensing range of this sensor was limited to 57% strain, it showed significantly enhanced sensitivity (GFs of $\sim$416 at 0 to 40% strain and $\sim$3667 at 48 to 57% strain), no frequency dependent sensing (frequency range 0.02–3 Hz), and excellent stability for 1000 stretching–releasing cycles at 7.5% strain.

Elastic conducting composite fibers

One attractive approach to fabricate textile strain sensors is to produce conducting elastomeric composite fibers by integrating conducting fillers within an elastomeric host using fiber fabrication techniques such as melt-spinning and wet-sinning (Fig. 4a and f). These techniques require that the conductive fillers are homogenously dispersed in the polymeric host. This is typically achieved in melt-spinning by using an extruder that mixes the two phases. In an early work, an elastomeric conducting composite fiber was fabricated by melt-compounding a thermoplastic elastomer (SEBS) and CB powder (up to 50 wt% loading) and then melt-extruding the composite material into a fiber (Fig. 4b).[5] The SEBS/CB fiber was attached to a fabric using a silicone film and used as a strain sensor (Fig. 4c). This composite fiber strain sensor showed sensing in the range of 20 to 80% strain with a GF of $\sim$20, a small resistance creep of $\sim$8.8% at a constant strain of 80%, and a low hysteresis of less than $\sim$7%. The sensing response of the composite fiber was also stable with $\sim$2.5% increase in resistance after $\sim$3800 stretching–releasing cycles and increasing the strain rate (from 4 to 48% s^{-1}) did not significantly affect its sensing performance. The sensor remained functional after two months or after washing eight times at 30 °C in a washing machine with a detergent. PU/MWCNT fibers were similarly produced by extruding the nanocomposite pellets (at 3 wt% MWCNT loading) using a single-screw extruder connected to melt pump and a circular die.[66] SEM observations revealed the presence of densely packed micron-size clusters (Fig. 4d), which are not desirable for achieving fiber strain sensors. The PU/MWCNT fiber extruded at 240 °C showed a conductivity of $\sim$0.03 S cm^{-1}. The sensing behavior was characterized by an increase in resistance when stretched to 10% strain. However, only partial recovery was observed after strain was released (Fig. 4e). Melt-spinning allows only limited incorporation of conductive fillers and typically leads to low conductivity. This is because the melt viscosity increases with the addition of filler and at high loadings, the viscosity will be too high for fiber extrusion. For instance, the spinnability of polycarbonate (PC)/MWCNT fibers deteriorated after 4 wt% MWCNT loading, whereby at 6 wt% MWCNT, it impossible to spin at high draw ratios.[67] Drawing during fiber spinning also plays an important role in the sensing performance of the fiber. For instance, for the PC/MWCNT fiber strain sensors, increasing the draw ratio from 4.8 to 12.0 resulted in GF enhancement; the GF $\sim$ 16 was measured for 3.5 wt% MWCNT loading and draw ratio of $\sim$8.

In wet-spinning, a formulation consisting of polymer host with conductive filler in an appropriate solvent is first prepared. Fibers are obtained by extruding the composite formulation into a coagulation bath. Many conductive fillers (*e.g.* PEDOT:PSS, CNT, GO, and AgNW) are versatile towards solution processing, making wet-spinning a useful technique for producing elastomeric conductive composite fibers for strain sensing application. As conducting fillers tend to aggregate less in dispersion than in melt, wet-spinning enables the production of homogeneous fibers with highly dispersed filler particles in the polymer phase, which is essential to achieve high strain sensing properties. Wet-spinning has been used to fabricate poly(styrene-*b*-isobutylene-*b*-styrene) (SIBS)/poly(3-hexylthiophene) (P3HT) composite fibers.[46] A maximum conductivity of $\sim$0.38 S cm^{-1} was achieved for SIBS/P3HT fiber with P3HT loading of $\sim$14 wt% when doped using tetrafluoroboric acid (HBF_4). The extremely high stretchability of SIBS ($\sim$1078%) remained greatly unaffected after the addition of $\sim$14 wt% P3HT loading exhibiting an elongation at break of $\sim$975%. The resistance of the SIBS/P3HT fiber increased up to a strain threshold of 550 to 770% after which it decreased with further stretching. In a cyclic stretching–releasing test with a strain amplitude of $\sim$12%, the fiber showed a GF of ~-1.6 and stable sensing response for 20 cycles. PU/PEDOT:SS conducting elastomeric composite fibers were also fabricated using the wet-spinning technique (Fig. 4g and i).[27] Fibers with conductivity of as high as 25 S cm^{-1} at $\sim$25 wt% PEDOT:PSS were reported. The PU/PEDOT:PSS fiber (with $\sim$13 wt% PEDOT:PSS loading) could sense strains of up to $\sim$260% with a GF of up to $\sim 10^4$ at 200% strain (Fig. 4j). When cyclically stretched and released

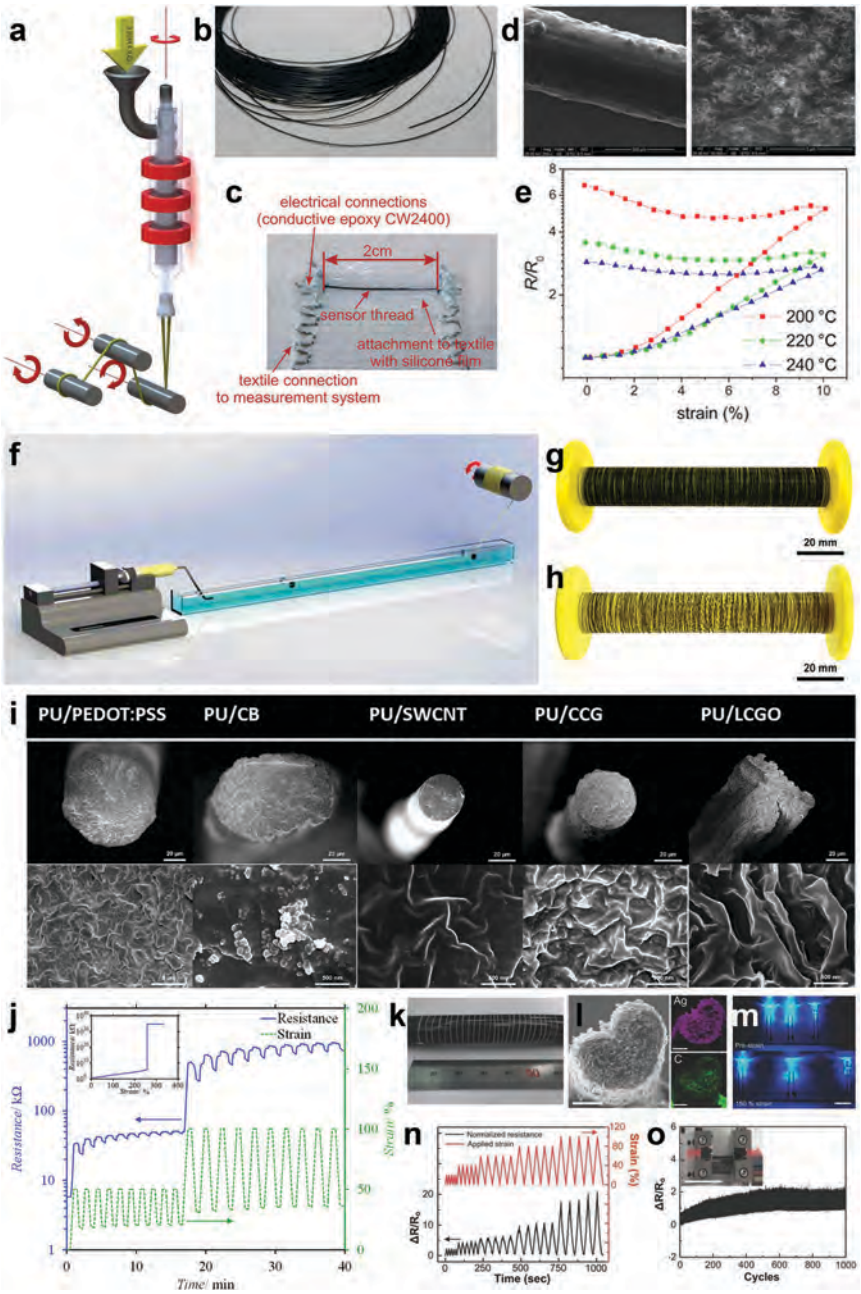

Fig. 4 (a) Schematic representation of melt-spinning process which can be used to fabricate fiber strain sensors. Adapted with permission.[126] Copyright 2016 Royal Society of Chemistry. (b) Photo of the melt-spun SEBS/CB composite fiber strain sensor and (c) after integration within a fabric.[5] (d) SEM images of lateral and cross-section surfaces and (e) strain sensing performance of the melt-spun PU/CNT composite fiber. Adapted with permission.[66] Copyright 2010 Royal Society of Chemistry. (f) Schematic representation of wet-spinning process used for fabricating fiber strain sensors. Adapted with permission.[126] Copyright 2016 Royal Society of Chemistry. (g) Photo of PU/PEDOT:PSS composite fiber on a spool. Adapted with permission.[27] Copyright 2014 John Wiley & Sons, Inc. (h) Photo of PU/LCGO fiber on a spool. Adapted with permission.[69] Copyright 2015 John Wiley & Sons, Inc. (i) Cross-section SEM images of various PU conducting elastomeric composite fiber strain sensors. Adapted with permission.[27] Copyright 2014 John Wiley & Sons, Inc. Adapted with permission.[69] Copyright 2015 John Wiley & Sons, Inc. Adapted with permission.[86] Copyright 2016 John Wiley & Sons, Inc. Adapted with permission.[70] Copyright 2016 IOP Publishing Ltd. (j) Strain sensing behavior of PU/PEDOT:PSS composite fiber. Adapted with permission.[27] Copyright 2014 John Wiley & Sons, Inc. (k–o) Fabrication and strain sensing performance of the SBS/AgNW–AgNP composite fiber: (k) photo and (l) cross-section SEM image, (m) images of LEDs connected to the fibers before and after stretching to 150% strains, (n) relative resistance change at various strains, and (o) stability of the sensor under cyclic stretching–releasing. Adapted with permission.[71] Copyright 2015 John Wiley & Sons, Inc.

to 100% strain, the composite fiber showed stable sensing after the first cycle. A wide range of other conducting elastomeric composite fibers such as PU/liquid crystalline GO (LCGO), PU/CB, PU/SWCNT, and PU/chemically converted graphene (CCG) fibers were produced with different sensing performance (Fig. 4h and i).[69,70,86] The PU/LCGO fiber showed electrical

conductivity (after thermal reduction) and sensing behavior at a very low percolation threshold of ~0.4 wt% GO, while ~16.7 wt% CB was required to impart conductivity and sensing to the fiber. The sensing range of these composite fibers varied from ~70% strain for PU/LCGO to ~40% strain for PU/CCG. While the PU/CB fiber showed the highest sensitivity (GF ~ 100 at 50% strain), its sensing behavior reversed at ~30% strain, *i.e.* resistance decreased with stretching for strains less than 30% and increased with stretching when strain was above 30%. These studies revealed that apart from the filler loading, the filler aspect ratio and the interaction of conducting fillers within the polymer matrix play critical roles in determining the strain sensing properties.[69,70,86]

Wet-spinning also enables the incorporation of high amount of conducting fillers within the fiber, which is useful for strain sensing application. For instance, highly conductive and stretchable composite fibers were produced by wet-spinning of SBS elastomeric polymer matrix containing ~75 wt% Ag nanoparticles (NP) and up to ~1.7 wt% AgNW (Fig. 4k and l).[71] The SBS/AgNW–AgNP composite fiber showed a very high electrical conductivity of up to ~2450 S cm^{-1} (at 1.7 wt% AgNW) while showing a high stretchability of ~900% at AgNW loading of ~0.6 wt%, which was only slightly lower than that of pure SBS fiber (~1182%). It was shown that when the SBS/AgNW–AgNP composite fibers were used to connect three LEDs to a power source, the LEDs remained illuminated even when the fibers were stretched to ~150% (Fig. 4m). This composite fiber showed a sensing range of ~100% strain and a GF of ~15 at 100% strain (Fig. 4n). During the 1000 stretching–releasing cycles at 10% strain, the sensing response initially increased to about 100% for the first 600 cycles before stabilizing (Fig. 4o). PU/AgNW composite fiber strain sensors with very high AgNW loading of up to ~76 wt% were also produced using wet-spinning, which showed an outstanding conductivity of ~14 205 S cm^{-1}, albeit with low stretchability (less than 3%).[72]

The fabrication of conducting and elastomeric composite fibers using the spinning techniques can be easily scaled up to produce strain sensing fibers and yarns that can be integrated into fabrics.[16] While composite fiber strain sensors typically have high sensitivity and sensing range, these sensors have low linearity and low cyclic stability.

Wrapping and buckling

Microstructural design is another way to enable strain sensing capability on elastic and non-conductive fibers. Creating surface structures through wrapping and buckling has been used to fabricate fiber strain sensors with high stretchability and high linearity. The buckling structure is usually achieved by wrapping or depositing solid-state conductive materials, *e.g.* CNT sheets or AgNWs, on pre-stretched elastic fibers. This method can be used to achieve both resistive and capacitive strain sensors on the fiber level. Once the buckling structure is formed, it can provide a stable conductance during deformation, which is suitable for capacitive strain sensing. The buckling structure has previously been used on films to fabricate stretchable conductive layers with stable conductance during deformation.[6,87,88]

This buckling structure was first realized on fiber by wrapping CNT sheets (NTS) on rubber fiber which was pre-stretched to typically 1400% strain.[29] The reversible short- and long-period buckling of CNT sheath occurred out-of-phase in the fiber axial and belt directions and provided a constant conductance during stretching. Additional SEBS and CNT layers were wrapped onto the fiber to realize capacitive strain sensing capability. This capacitive type NTS@rubber@NTS@fiber sensor showed 860% increase in capacitance when stretched to 950% strain (GF ~ 0.91). It also showed a linear response (up to 950% strain) and a high cyclic stretching–releasing stability over 500 cycles (at 950% strain). However, the large diameter (2 mm) of the rubber core led to a high core-to-sheath volume ratio, which resulted in a low overall conductivity and required a large driving force to activate the strain sensor. A downsized fiber sensor (as thin as 40 μm) was then developed, which required lower drive force to activate the strain sensor while maintaining high stretchability (sensing range) and high stability.[83] Here, small-diameter SEBS and plasticizer mixed rubber fiber was fabricated using a melt-drawing method and was used as the core fiber (Fig. 5a). The strain on the fiber was characterized by the change in capacitance between the two NTS layers during elongation (Fig. 5b). A 4 cm-long downsized fiber strain sensor showed a 119% linear increase in capacitance (GF ~ 0.6) at 200% strain. It also had negligible hysteresis and excellent cyclic stability (1000 stretching–releasing cycles at 100% strain and 5000 cycles at 40% strain).

The buckling method can also be used to fabricate resistive strain sensor fibers. For instance, a bi-sheath buckling structure was formed by spray-coating a thin strain-gauge-enhancement rubber layer between the NTS and the rubber core (NTS@rubber@fiber) to make a resistive-type sensor.[22] This sensor exhibited very large strain range (up to 600%), high linearity (two linear ranges: GF of ~0.5 for strain in the range of 0 to 200% and GF of ~0.14 for strain in the range of 200 to 600%), fast response (~80 ms) and fast recovery (5 s), excellent stability, and almost no hysteresis for 5000 stretching–releasing cycles at various strains from 100% to 600%. In addition, this sensor also showed high sensitivity to twist insertion. Under a constant tensile stress of 64 kPa, the resistance of the fiber increased linearly by 14% when a total of 2.2 turn cm^{-1} twist was inserted, which corresponds to ~0.004% per degree.

Other geometric designs on the buckling structure have also been explored. A sandwich-structured fiber was fabricated by applying NTS on two opposite sides of a pre-stretched (to 300%) rectangular silicone rubber fiber (Fig. 5e and f).[30] This sandwich fiber provided almost constant electrical conductance after 200 cycles of stretching (up to 200% strain), twisting (up to 1700 rad m^{-1}), and bending (up to 150°) (Fig. 5g and h). A linear relationship between capacitance and tensile strain, negligible hysteresis, and high cyclic stretching–releasing stability were observed (Fig. 5h). Its sensitivity to other deformations enabled other functionalities such as torsional sensing and supercapacitor.

AgNW/PU composite were also used to fabricate PU fibers with the buckled surface morphology (Fig. 5c and d).[74] This conductive fiber possessed a high conductivity (up to ~1.4×10^4 S cm^{-1}) and good stretchability (up to 400%). While ultrasonic treatment in

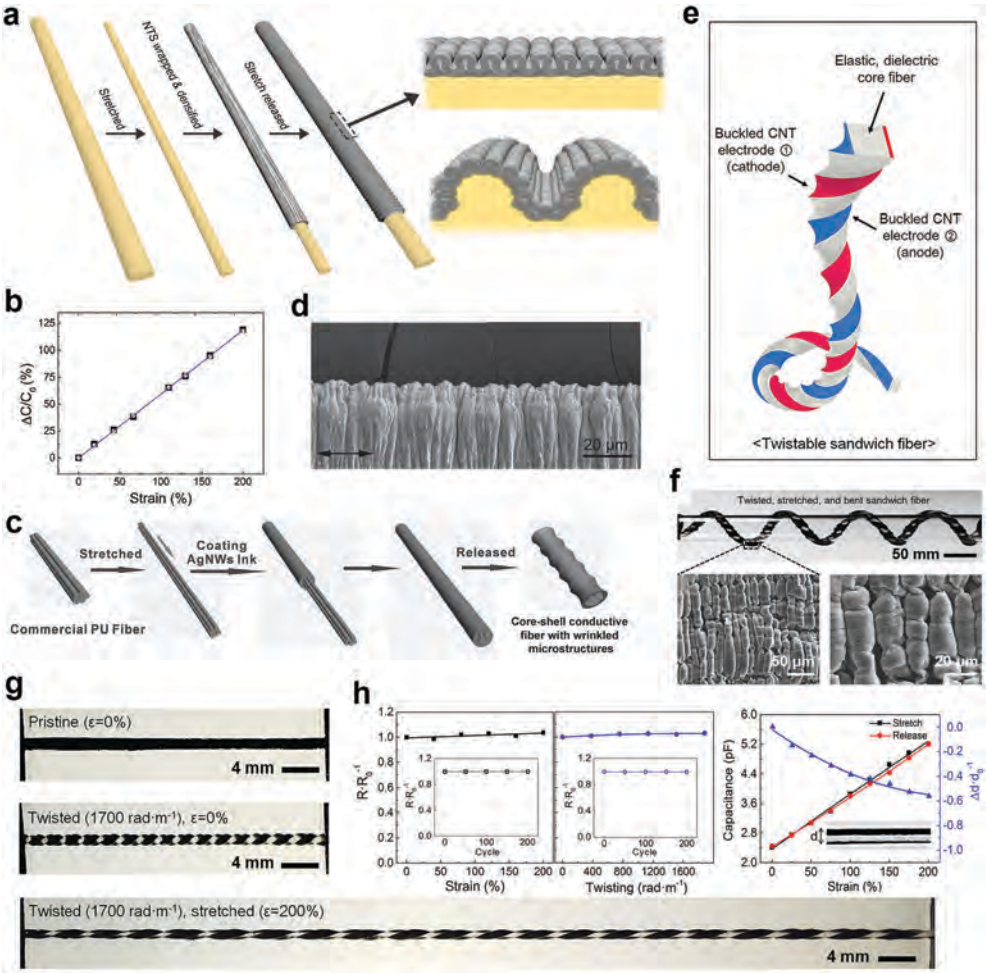

Fig. 5 (a) Schematic illustration showing the fabrication process of an NTS@rubber fiber, and the buckling structural for downsized fiber core (top) and the hierarchical buckling on millimeter–diameter fibers (bottom). (b) Dependence of NTS@rubber@NTS@fiber sensor capacitance on strain during stretching (solid square) and stretch release (open circles), where the blue line is a linear fit of the data. Adapted with permission.[83] Copyright 2016 John Wiley & Sons, Inc. (c) Schematic illustration of the fabrication of AgNW coated stretchable conductive core–shell fibers with buckling microstructures. (d) SEM images showing the wrinkled microstructures of the AgNWs coating. Adapted with permission.[74] Copyright 2016 John Wiley & Sons, Inc. (e) Schematic illustration of a twisted sandwiched fiber with a rubber core and two symmetric buckled CNT electrodes. (f) Photograph showing a twisted sandwiched fiber wound around a glass rod and SEM images showing microscopic CNT buckles. (g) Photographs of the sandwich fibers that are released, twisted to 1700 rad m^{-1}, and twisted to 1700 rad m^{-1} and stretched to 200% strain. (h) Resistance change as a function of tensile strain and twist insertion, and capacitance and change in fiber thickness *versus* tensile strain of the sandwiched fiber. Adapted with permission.[30] Copyright 2016 American Chemical Society.

water for 1200 s increased the fiber resistance by ~500%, it was still possible to use it as a strain sensor. Flexible piezoresistive fibers were prepared by twisting multiple fibers together, which exhibited sensitivity to pressure and bending deformations (0.12 kPa^{-1} and 0.012 rad^{-1}). This fiber sensor showed a low detection limit, and a high cyclic stability (no resistance change under 100% strain for 4000 stretching–releasing cycles). As seen above, while wrapping and bucking are effective strategies to achieve highly stable and linear sensors, they typically lead to low sensitivity (GF). Moreover, the complicated and multi-step fabrication process impose challenges in achieving fiber strain sensors that are longer than a few centimeters.

Twist, helix, and coil insertions

Creating helical structure on fiber scale is another way to impart stretchability on rigid fibers or fibers with low elasticity. This is often achieved by overtwisting or coiling a straight fiber. When a coiled fiber is stretched, deformation is accommodated by the helical structure, which minimizes the strain imposed on the fiber. Constructing coiled fiber from conductive materials has enabled many applications such as stretchable conductive wires,[75] actuators,[89,90] and strain sensors.[28,76,82] Spring-like (full-helical) SWCNT yarn strain sensors were produced by over-twisting a thin film of CVD-grown SWCNTs (Fig. 6a).[75] The electrical conductivity of helical SWCNT yarns reached ~440 S cm^{-1} at the unstretched state and breaking strain was ~285%. By employing a similar approach with controlled coiling position, a SWCNT yarn composed of a helical segment and two straight ends were produced (Fig. 6b).[28] This partial-helical yarn showed an improved elasticity compared to the full-helical counterpart as a result of more uniform loops and less defects. The resistance of partial-helical[28] yarn strain sensor increased with

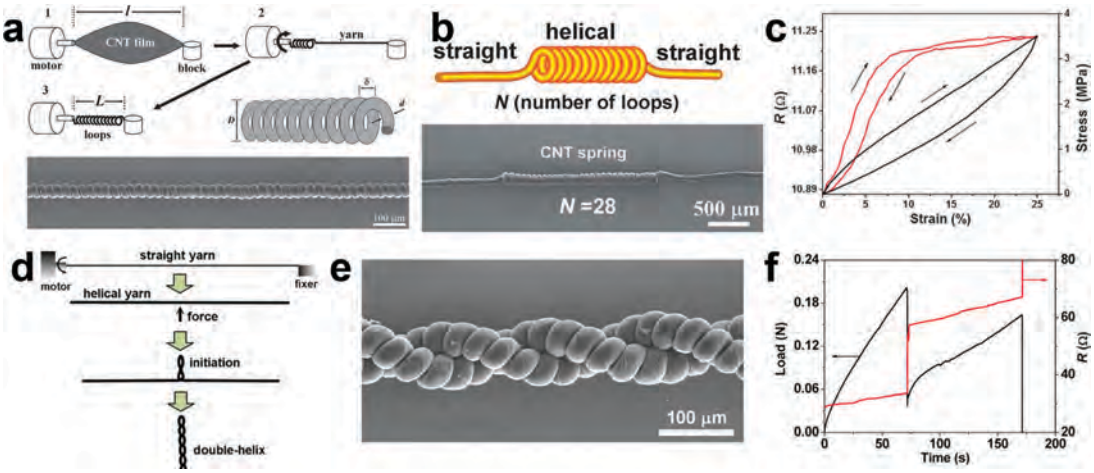

Fig. 6 (a) Schematic illustration of the coiling process of a SWCNT sheet into a helical yarn and the corresponding SEM image of the helical yarn strain sensor. Adapted with permission.[75] Copyright 2012 John Wiley & Sons, Inc. (b) Schematic and SEM image and (c) strain sensing property of partial-helical SWCNT yarn. Adapted with permission.[28] Copyright 2013 Royal Society of Chemistry. (d) Schematic illustration of the fabrication process of a double-helix SWCNT yarn and its corresponding (e) SEM image and (f) strain sensing property. Adapted with permission.[91] Copyright 2013 American Chemical Society.

strain (up to 25%) with high stability over 1000 stretching cycles. The rate of resistance change, however, was not constant in the partial-helical SWCNT yarn and more rapid resistance changes were observed at low strains ($\leq$5%) resulting in the GF of $\sim$0.14 and $\sim$0.03 for strain ranges of 0 to 5% and 5 to 25%, respectively (Fig. 6c).

Double-helix SWCNT yarn strain sensors were also fabricated by first twisting a SWCNT film into a yarn by an electric motor, over-twisting into a single-helical yarn, and then applying a force in the middle section which triggered the rotation and mutual entanglement of the two yarn segments from both sides (Fig. 6d and e).[91] This double-helix SWCNT yarn showed an abrupt change in resistance (Fig. 6f) when the first yarn ruptured (at 50–100% strain) after which the resistance increased further until failure (150–200% strain). In another report, a highly stretchable coiled CNT yarn was fabricated by over-twisting straight CNT yarn, which showed dramatically improved stretchability (up to 985% *vs.* 6.8% for neat CNT yarn).[76] This entangled coiled CNT yarn showed a large sensing range (up to 500% strain), positive GF ($\sim$0.13 at a strain of 500%) and high cyclic stretching–releasing stability (600 cycles at 500% strain).[76] However, the stress fluctuated during stretching, which had a negative effect on the sensitivity and stability of the fiber strain sensor. While coiling is relatively easy to achieve (compared to buckling, for instance) and scale-up, the sensitivity of the coiled yarn strain sensors is typically low (GFs $<$ 0.5)[28,76,82] and the strain range is usually less than the maximum stretchability of the yarn. Coiling produces sensors with high cyclic stability, although some non-linearity in the sensing response is inevitable.

Coaxial fibers

Fiber strain sensors could be achieved by using core–shell structures. These fiber strain sensors typically consist of a conductive core covered by an elastic shell. In this design, an important requirement for the core is stretchability and conductivity. The fiber core should be able to accommodate large stretch deformation while remaining conductive. Suitable materials such as liquid metals (LMs), ionic liquids (ILs) and carbon/elastomer composites have been explored to fabricate the fiber core. Coaxial structures can be used to produce both resistive and capacitive fiber strain sensors. These coaxial fibers have been fabricated by liquid injection, wet-spinning, or printing.[32,77,78]

It was demonstrated that a low melting point eutectic indium-gallium (EGaIn) LM can be injected into hollow SEBS fiber to form a highly stretchable conductive fiber.[77] This EGaIn@SEBS fiber showed similar breaking strain to pure SEBS fiber (up to 1000%) while retaining high electrical conductivity even when stretched to large strains and after hundreds of stretching–releasing cycles. The conductivity of the EGaIn@SEBS fiber ($\sim 3.3 \times 10^4$ S cm^{-1}) was higher than any conductive composite fibers. Although this fiber showed an increase in resistance when compressed (*i.e.* pinching) due to the deformation of the LM core, the authors did not evaluate its strain sensing application. A stretchable LM-PDMS fiber filled with eutectic indium-gallium-tin (EGaInSn) showed an excellent stretchability up to 140% strain similar to pure PDMS fiber and a linear change in resistance with applied strain.[78] The sensitivity of this fiber could be regulated by channel sizes *i.e.* GF increased from $\sim$2.2 to $\sim$3.4 when fiber diameter decreased from 750 to 500 μm. The fiber-based strain sensors also showed almost no hysteresis ($\sim$0.11%), a low detection limit (0.3% strain), large sensing range (up to 140% strain), and high stability (over 3500 cycles). In another report, a pair of EGaIn-filled Hytrel fibers were intertwined into a double helix structure to create capacitive sensors that were sensitive to torsion, touch, and strain.[32] The maximum GF was $\sim$0.82 (at 100% strain) and the lowest detection limit was 2.9%.

Other types of materials such as graphene-based and CNT-based composites were fabricated into a core-sheath conductive

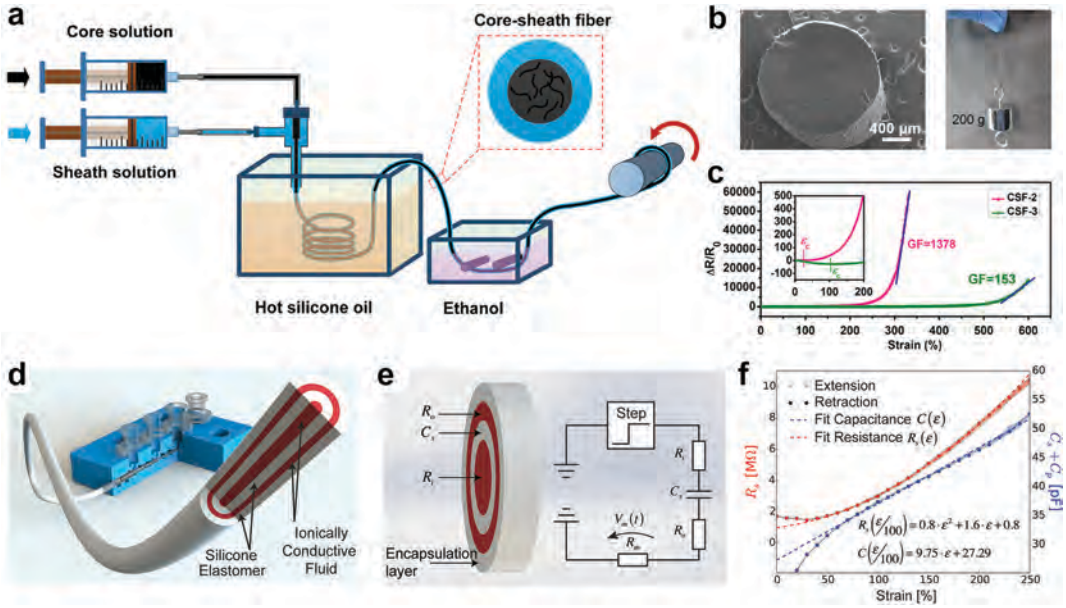

Fig. 7 (a) Schematic illustration of the coaxial wet-spinning process for the highly stretchable fibers. (b) SEM image showing the cross-section of the core-sheath fiber with 2 wt% MWCNT, and photograph of a knotted fiber (diameter 1.7 mm) carrying a weight of 200 g. (c) Resistance change ($\Delta R/R_0$) as a function of the applied strain on CNT yarn with 2 and 3 wt% CNT loading. Adapted with permission.[80] Copyright 2018 American Chemical Society. (d) Schematic illustration of multicore–shell printing process and the resulting fiber. (e) Illustration of the sensor cross-section and equivalent circuit diagram of the readout circuitry for a capacitive strain sensor. (f) Model predictions and experimental results of the resistance and total capacitance of the sensor up to 250% strain. Adapted with permission.[84] Copyright 2015 John Wiley & Sons, Inc.

fiber structure. For instance, wet-spun Silicone elastomer-protected MWCNT fiber was produced (Fig. 7a and b).[80] The MWCNT infused elastomer served as the resistive sensing core while the outer layer served as the insulating sheath. At 2 wt% CNT, the fiber was stretchable (>300%) and washable where the resistance changed 15% after 11 washing cycles. As a strain sensor, it sustained >10 000 cycles under 100% strain and displayed fast response and low hysteresis. Its resistance was also stable at various room temperature and humidity conditions but the resistance dropped by ~80% when heated to 100 °C. This fiber also exhibited high sensitivity with a GF of ~0.68 at 50 to 100% strain and ~1378 at 300 to 330% strain (Fig. 7c). However, such a large variation of GF with strain (indicating non-linearity) is not desirable for practical applications.

Hollow fibers with ionic liquid (IL)-filled channels have also been produced.[82] Straight and coiled copper wires were used as templates to create hollow PDMS fibers with straight or helical channels. The fibers were fabricated *via* a "fill and seal" process in which the IL (1-ethyl-3-methylimidazolium tetrafluoroborate, $EMIMBF_4$) was injected into the channel of the hollow fiber. The conductive fibers were stretchable up to 230% and could sustain 10 000 stretching–releasing cycles. The fiber with a straight channel showed an increase in resistance with applied strain of up to 100%, giving rise to GFs of 2.0 to 2.8. It demonstrated fast response even at different frequencies of 1 to 10 Hz. In comparison, the fiber with helical channel showed low change in resistance even at 100% strain (GF < 0.5). Coaxial structures can be used to achieve multiple electrode, dielectric, and encapsulation layers, which are necessary in fabricating capacitive strain sensors, in one-step. For instance, a capacitive fiber strain sensor was achieved by constructing a multicore–shell fiber using a printing method.[84] The fiber consisted of four concentric layers including two ionically conductive layers as the conductors, and two silicone elastomer layers that served as the dielectric layer and encapsulation (Fig. 7d and e). This fiber showed strain sensing capability up to 250% strain with ~9.75 pF capacitance change per 100% strain, which corresponded to a GF of ~0.35 (Fig. 7f). The dynamic sensor response could be accurately tracked over a range of applied strain frequencies and amplitudes (up to 150% strain). However, this fiber was susceptible to environmental conditions that affected conductivity, sensor output, and fiber stiffness. Coaxial structures offer great flexibility in producing resistive and capacitive fiber strain sensors with high sensitivity, sensing range, and/or stability, although achieving high overall sensing performance can be challenging.

Knitting, weaving, or braiding

Fabric strain sensors have been produced by knitting conductive fibers or yarns. Such fabric strain sensors are preferred structures for wearable applications. Early fabric strain sensors were produced by knitting steel yarns or carbon fiber yarns into tubular plain-knitted fabrics (Fig. 8a).[92] While highly conducting, these fabrics showed limited sensing range of up to 20% strain. The resistance of the knitted fabrics decreased with stretching along the wale direction (shown in Fig. 8j) with GF of up to ~−4. Both fabrics showed hysteresis in 5 stretching–releasing cycles at 20% strain; the resistance of the steel-based fabric increased with stretching cycles. Interestingly, the sensing behavior of the carbon fiber-based fabric, remained unchanged

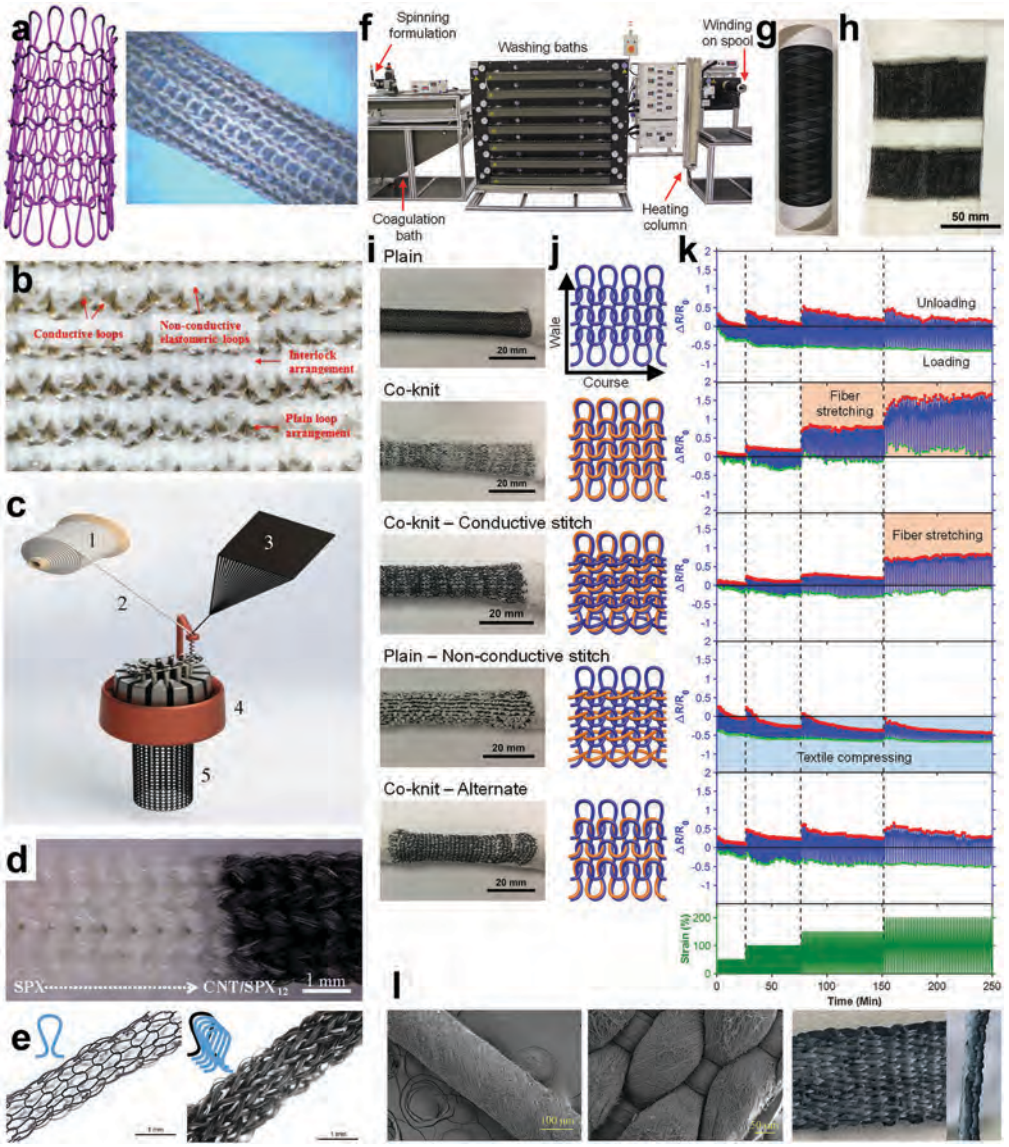

Fig. 8 (a) Schematic illustration a tubular knitted fabric and optical image of a knitted steel yarn. Adapted with permission.[92] Copyright 2005 Elsevier Ltd. (b) Fabric strain sensor made by co-knitting silver-plated nylon and elastomeric yarns.[23] (c) Schematic illustration of the fabrication process and (d) photograph of knitted strain sensor fabric based on CNT sheath/spandex core yarn (CNT/SPX). Adapted with permission.[17] Copyright 2016 American Chemical Society. (e) Fabric strain sensors made by knitting PU/PEDOT:PSS composite monofilament into a plain-knit and a co-knit consisting of four-ply PU/PEDOT:PSS monofilaments and a commercial Spandex yarn. Adapted with permission.[16] Copyright 2015 American Chemical Society. (f) Photograph of the fiber wet-spinning of (g) PU/PEDOT:PSS multifilaments that were knitted into (h) a wearable fabric strain sensor and (i) fabric prototypes. (j) Schematic illustrations and (k) strain sensing properties of the various knitted structures obtained from PU/PEDOT:PSS multifilaments. Adapted with permission.[19] Copyright 2018 Elsevier Ltd. (l) SEM and optical images of PEDOT-coated nanofiber yarns woven into a fabric pressure sensor. Adapted with permission.[93] Copyright 2017 Nature Publishing Group.

even when the temperature was increased to 200 °C. Fabric strain sensors were also achieved by knitting silver-coated conductive nylon yarns in an alternate pattern with insulating core-spun Lycra yarns (Fig. 8b).[23] When stretched to a maximum strain of 40% in the course direction, the fabrics showed GFs that ranged from 0.08 to 2.5. The sensing range decreased when the insulating yarn thickness increased from 156 to 800 dtex (mass of yarn in grams per 10 000 meters). This result illustrates that it is possible to tailor sensing properties with knitting patterns.

A fabric strain sensor was fabricated by continuously wrapping CNTs around Spandex yarns during knitting (Fig. 8c and d).[17] The fabric with ~9 wt% CNT showed strain sensing range of up to 100% with a GF of ~0.4. There was only less than 2.3% decrease in sensitivity and a small hysteresis after 1000 stretching–releasing cycles at 100% strain. PU/PEDOT:PSS monofilaments were knitted with Spandex yarns to make tubular fabrics with a sensing range of up to ~160% strain (Fig. 8e).[16] The resistance of the fabric decreased with stretching. The sensitivity of the fabric increased with the number of filaments used, reaching the

highest GF of ~ -1 with four filaments. The sensing response was stable during ~ 500 stretch–release cycles and was further improved by co-knitting with a Spandex yarn. These works demonstrated the potential use of knitted textiles in wearable application by using specially-designed supporting frames.

Self-supporting fabrics, *i.e.* those that can be worn directly without the need for a supporting frame, substrate, or an additional clothing item, are required to realize truly wearable strain sensors. This can be achieved through a scalable fiber fabrication that provides suitable mechanical properties for conventional textile processing. Using a medium-scale wet-spinning line (Fig. 8f), the production of PU/PEDOT:PSS multifilaments was recently demonstrated in kilometer scale (Fig. 8g). The fabric strain sensors (Fig. 8h–j) with five elaborate knit patterns (*i.e.* plain knit, co-knit, co-knit with conductive stitch, plain knit with non-conductive stitch, and co-knit alternate)[19,20] showed that the sensing performance can be tailored using alterations in the loop configurations and stitch insertions (Fig. 8i–k). All fabrics could sense strains as large as 200%. The plain-knit fabric showed a GF of ~ -0.7 at 50% strain. In cyclic stretch–release tests at 100% strain for 500 cycles, the fabrics showed stable sensing response after ~ 50 cycles. The strain sensing behavior of the knit prototypes was demonstrated in a self-supporting wearable fabric consisting of two ~ 5 cm $\times$ 10 cm knitted strips of PU/PEDOT:PSS multifilaments within a ~ 15 cm $\times$ 10 cm plain knit fabric.

Using two layers of silver-plated knitted fabric as electrodes and silicone elastomer as a dielectric layer, a capacitive fabric strain sensor was achieved.[31] Fabric sensors with desired shape were created by laser cutting, which showed linear strain–capacitance relationship (GF $\sim$ 1.23) and low hysteresis when cyclically stretched to 100% strain. Nevertheless, a 12% decrease in capacitance output was observed in 1000 stretch–release cycles at 100% strain. It was shown that this fabric strain sensor could be integrated in/onto garments (*e.g.* gloves) for wearable applications. With woven fabric pressure sensors having been developed (Fig. 8l),[93] it is expected that weaving can also be used to achieve fabric strain sensors. Braiding has also shown potential in fabricating piezoelectric textile strain sensors.[94] Knitting, weaving, and braiding enable the production of fabric strain sensors that are truly wearable. These methods offer numerous means to achieve fabrics with desired sensing performance, by changing the fabric pattern, the number of conducting threads, and the properties of the yarn used in co-knitting or co-weaving.

Strain sensing mechanisms

The sensing mechanisms in textile strain sensors depend on the structure of the textile component (fiber, yarn, or fabric), fabrication approach, and the stretchable and the sensing components used in the textile sensor. The sensing response of a textile strain sensor is determined by the interplay of four main factors: (1) inherent variation in the properties (*e.g.* resistance) of the individual sensing component with strain, (2) crack formation in the sensing layer, (3) changes in the conduction network, and (4) geometrical transformation of the textile assembly.[39,48] These four factors are discussed in detail in this section.

Properties of the sensing component

The stretching-induced increase in resistance of individual CNTs as the result of increase in the band gap energy,[95] was found to be responsible for the increase in resistance of CNT yarns upon stretching.[48,64] As opposed to composites where individual CNTs have limited contacts, in a pure CNT yarn, CNTs are tightly packed. Thus, stretching the CNT yarn has negligible effect on the electrical conduction network. In this case, the sensing properties comes primarily from the changes in the resistance of individual CNTs in the yarn upon stretching.[48]

In Au/ZnO NW coated carbon fiber piezoelectric strain sensor, the electrical transport property was found dependent upon the changes in the band structure of ZnO and the piezoelectric potential when strain was applied.[33] Here, the changes in ZnO band structure, characterized by the changes in its electron affinity, produced a piezoresistive effect. In addition, the piezoelectric polarization produced surface charges at the Au/ZnO contact interface, which led to the changes in the Schottky barrier height. These characteristic changes in piezoresistive properties were also observed for NW@CNT/rGO coated fabric.[44] Interestingly, the piezoresistive properties of ZnO could be tailored through microstructural changes in the crystal size, orientation, morphology, aspect ratio and crystalline density.

Crack formation

When sensing materials are coated on a textile-based substrate, the sensing layer can crack during deformations because of the mechanical property mismatch between the two components. These crack formations lead to resistance increase and can also be harnessed for strain sensing. Detailed *in situ* SEM observation of the PPy-coated Lycra fabric revealed the formation of micro-cracks (perpendicular to the stretch direction) in the PPy layer, which increased in number, width, and length with stretching.[58] The strain sensing property of the PPy-coated fabrics resulted from micro-cracks opening (when stretched) and closing (when released) (Fig. 9a).[96] Similarly, when the graphite-coated silk fibers were subjected to tensile strain, the decrease in the overlapping area between the coated graphite flakes led to an increase in resistance and the contact restored upon strain release.[61] This phenomenon was also observed for ZnO NW coated PU fibers (Fig. 9b and c),[62] coaxial elastomer-wrapped CNT fibers (Fig. 9d),[81] graphene-coated PU yarns,[97] AgNW coated single covered yarn (SCY),[98] and knitted CNT/Spandex yarns.[17]

While crack formation results in distinct variation of the sensing response and high sensitivity (GF), it typically leads to low sensing range, hysteresis, non-linear sensing, and low cyclic stability. The irreversible crack formation throughout GWF upon initial stretching caused an exponential rise in resistance (Fig. 9e and f).[99] Due to the nature of crack formation mechanism,

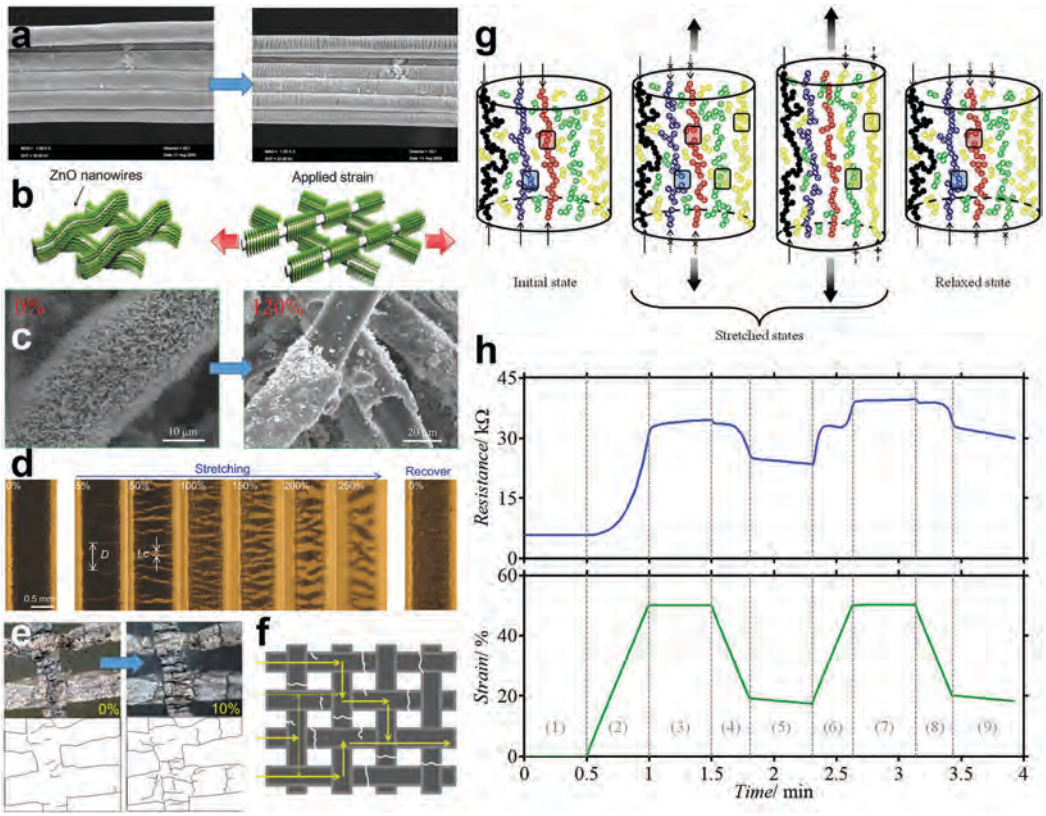

Fig. 9 (a) SEM images of PPy-coated PU fibers before and after stretching to 110% strain showing crack formation of the coating layer. Adapted with permission.[96] Copyright 2006 Elsevier Ltd. (b) Schematic illustration and (c) SEM images of ZnO NW coated PU fiber strain sensor showing the formation of cracks and flaking off of the coating layer upon stretching. Adapted with permission.[62] Copyright 2016 John Wiley & Sons, Inc. (d) Images of crack formation of the inner conducting layer when elastomer-wrapped CNT coaxial fiber was stretched from to 250% strain. Adapted with permission.[81] Copyright 2018 John Wiley & Sons, Inc. (e) Optical images showing the formation of crack in GWF strain sensor under strain and the corresponding schematic illustrations and (f) schematic representation of the current pathway through a fractured GWF. Adapted with permission.[99] Copyright 2012 Nature Publishing Group. (g) Schematic illustration of structural rearrangement of filler particle networks inside an elastomeric host for a composite fiber and (h) resistance change with strain for a representative PU/PEDOT:PSS composite fiber within two initial stretching–releasing cycles. Adapted with permission.[27] Copyright 2014 John Wiley & Sons, Inc.

the sensing range was limited to only 8% strain. Crack formation resulted in a non-linear resistance response and considerable hysteresis when GWF strain sensor was repeatedly stretched.[40] For the AgNW coated SCY yarn, when the applied strain increased beyond the pre-cracked strain of 40%, the irrecoverable damage to the AgNW network led to increase in resistance.[98] For the PEDOT:PSS/graphene-coated cotton fabric, the crack-induced sensing resulted in 20% and 70% increases in resistance after the first 2 and 20 stretch–release cycles, respectively.[100] It was found that increasing the sensing layer thickness (*e.g.* by increasing the number of coating) reduced the stability of the sensing response due to the non-uniformity of micro-cracks.[97] Nevertheless, it is possible to achieve excellent cyclic stability by controlling the crack formation on the sensing layer for instance by using pre-cracked fiber with a helical microstructure.[98]

Alteration of conduction network

In resistive textile strain sensors, the sensing performance can be explained by the changes in the conduction network upon stretching. From percolation theory, there is a minimum amount of conducting filler required to establish conducting paths in an insulating host.[101] Often, the weak interaction between the filler and the host leads to the disconnection of conductive paths upon stretching, resulting in resistance increase. For conducting elastomeric composite fibers, five types of conducting networks have been proposed (Fig. 9g):

1. Unbreakable networks that remain uninterrupted under strain (●)
2. Reversible networks that break with strain but restore when strain is removed (◉)
3. Irreversible networks that if broken, are not recovered when strain is released (◉)
4. Isolated networks that cannot form conductive networks on their own (◉)
5. Debonded networks that can form conductive networks with strain (◉).[27]

The interruption, deformation or re-arrangement of the above conductive filler networks during the strain and release periods as a result of their slippage, debonding and reversibility were found to determine the resistance response of the composite fiber.[27] In PU/PEDOT:PSS fiber, while stretching generally

resulted in disruption of reversible and irreversible conducting networks, it was observed that it was possible for the debonded networks to connect and for the isolated networks to form contacts with other networks, thereby decreasing the fiber resistance (Fig. 9h).[27] The stretching-induced disruption of conducting network also increased the resistance of SBS/AgNW–AgNP,[71] PU/rGO,[86] PU/CNT,[70] and PU/CCG[70] composite fibers, and CB/CNC/NR coated PU yarn.[45] For the SIBS/P3HT composite fiber, strain-induced contacting of P3HT chains was found to take place at high strain region of $>700\%$ resulting in a decrease in resistance.[46]

In composite systems, tunneling-assisted hopping between neighboring fillers at loadings lower than percolation threshold can also change with strain. One such example is the strain-dependent resistance property of the PC/CNT spray-coated PET fabric.[54] Since the CNT has lower resistance than the PC matrix, charge tunneling could take place between adjacent CNTs. The inter-CNT gaps increased with stretching and so as the sensor resistance.

Stretching also induces alignment of conducting fillers to from the conductive network. For example, the decrease in resistance of the PPy-coated Lycra fabric with stretching was attributed to the improved alignment of the PPy chains.[9] For PEDOT:PSS-soaked Spandex fabric, the combined effects of alignment and damages in the conductive network resulted in the increase and decrease in conductivity at the respective stretched and relaxed states.[51] In PEDOT:PSS-printed fabric, stretching gave rise to enhanced conductivity due to increased contact between the PEDOT:PSS chains that penetrated inside the fabric.[56] Here, stretching of the fabric resulted in compression of the yarn and promoted fiber contact. Similar observations were made for rGO-coated fabric that showed a decrease in resistance when stretched above 33%.[18]

Alteration of the conductive network sensing mechanism typically leads to large changes in resistance with stretching and thus result in textile strain sensors with high sensitivity (large GF). These textile strain sensors can sense large strains beyond 100%.[27,46,71] However, stretch-induced conductive network changes gives rise to noticeable hysteresis, non-linear sensing response, and limited cyclic stability. For the PEDOT:PSS coated Spandex fabric, since the conductive network did not recover when the strain was released, a considerable hysteresis in the conductivity was observed during the cyclic stretch–release test.[51] The permanent loss of irreversible network with stretching resulted in a sudden rise in the resistance of the PU/PEDOT:PSS composite fibers in the first cycle,[27] and caused $\sim$100% increase in resistance for the SBS/AgNW–AgNP fiber after 600 cycles.[71]

Geometrical transformations

Upon stretching materials in one direction, the shape of the material in the traverse direction will change with respect to its Poisson's ratio. This geometrical changes are key to controlling the strain sensing properties of some resistive and capacitive textile-based strain sensors. In the case of the resistive textile-based sensors, the changes in length (L) and cross-section area (A) with stretching result in changes in the resistance (R) of the sensor according to eqn (1). When sensing is only attributed to geometrical changes in the sensor, the resistivity (ρ) remains constant at all stretching conditions.

For capacitive textile-based sensors that are composed of a dielectric layer (with length l_0, width w_0 and thickness d_0) sandwiched between two electrodes, stretching in the length (l) direction results in changes in width (w) and thickness (d) of the dielectric layer according to eqn (5) and (6). These geometrical changes will result in changes in capacitance (C) of the textile sensor (eqn (7) and (8)) with strain (ε).[30]

$$w/w_0 = (l/l_0)^{1/2} \quad (5)$$

$$d/d_0 = (l/l_0)^{1/2} \quad (6)$$

$$C/C_0 = lwd_0/l_0w_0d \quad (7)$$

$$\Delta C/C_0 = \Delta l/l_0 = \varepsilon \quad (8)$$

For carbon fibers, the changes in the dimension of the fiber during stretching (*i.e.* decrease in fiber diameter) were responsible for the changes in resistance response and variations of fiber resistivity because of microstructural deformation was negligible.[63] Geometrical transformation was the main mechanism for the increase in the electrical resistance of liquid metal filled hollow fibers with stretching (Fig. 10a and b).[77,78] As theoretical predictions suggested, the increase in the resistance of the fiber was proportional to the change in the square of the length. For highly conductive coiled CNT yarn strain sensors, the change in resistance was dominated by spring deformation (geometrical transformation) as opposed to CNT sliding (Fig. 10c).[28] Stretch-induced geometrical transformation in double-helix CNT yarns resulted in reduced contact area between the closely-packed helical loops and increased yarn resistance.[91] In rGO-coated PDCY strain sensor, the geometrical transformation increased the resistance with stretching. This effect was the result of filament separation in both inner and outer layers as well as the decreased contact area (increased contact resistance) between these layers (Fig. 10d and e).[25]

The mechanism of strain sensing in fabrics are more complicated than fibers and yarns. Stretching can alter the arrangement of conducting fibers or yarns within the fabric and change its electrical properties. The geometrical transformation of fabrics under strain will vary greatly depending on the number and arrangement of conducting fibers or yarns (*e.g.* knitting patterns, whether the conductive fiber or yarn is co-knitted together with non-conductive yarns) and the direction of stretching (*e.g.* course or wale directions in knits).[16,19,23,92,102] Apart from the geometrical changes, it is also possible that applying strain on a fabric can stretch individual fibers or yarns and change their electrical properties through other mechanisms (*e.g.* alteration of conducting network).[16,19] In a simple plain knit fabric composed of only conducting fibers, two types of electrical resistance determine the overall equivalent resistance of the fabric: the length-related resistance (R_l) of the fiber between the loop interconnects and the contact resistance (R_c) between the two interlocked fibers (Fig. 10f).[92,102] Stretching the fabric

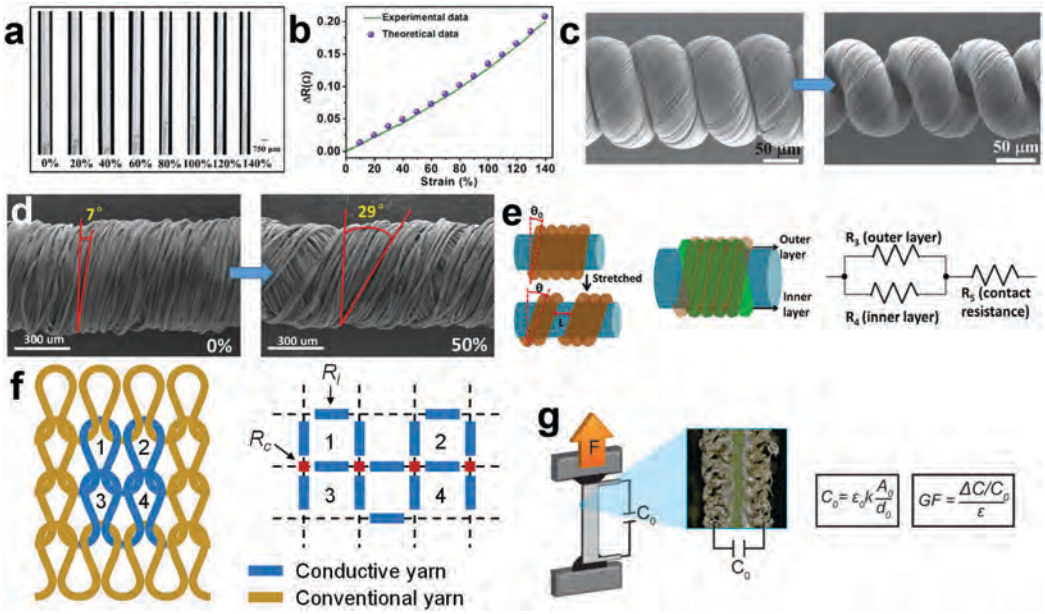

Fig. 10 (a) Images of liquid metal-filled fiber strain sensor which show shrinkage of the inner channel in response to the strain and (b) agreement of experimentally measured resistance response with theoretical prediction. Adapted with permission.[78] Copyright 2017 Royal Society of Chemistry. (c) SEM images of a coiled CNT yarn strain sensor before and after stretching showing separation of loops. Adapted with permission.[28] Copyright 2013 Royal Society of Chemistry. (d) SEM images of rGO–PDCY yarn strain sensors before and after stretching and (e) schematic illustration of the structural changes of the yarn during stretching. Adapted with permission.[25] Copyright 2015 John Wiley & Sons, Inc. (f) Schematic illustration of conducting loops in a knitted fabric and the corresponding equivalent circuit diagram (R_l: length-related resistance and R_c: interlocking contact resistance). (g) Cross-sectional image of a textile-based capacitive strain sensor and relationships showing how changes in capacitance relate to geometrical transformation of the dielectric layer. Adapted with permission.[31] Copyright 2017 John Wiley & Sons, Inc.

changes R_l by relocating the interlocking points between adjacent loops and also modifies R_c according to Holm's theory[103] (eqn (9)). Studies have shown that the contact resistance between the interlocked fibers or yarns (R_c) determines the sensing properties of the knitted fabrics.[92] Assuming that individual fibers are not stretched, the resistivity (ρ) and hardness (H) of the fiber will remain unchanged under strain. Stretching along the wale direction of the knit increases the contact pressure (P) and the number of contact points (n) between the conducting fibers at the interlocks and decreases R_c.[16,19] In contrast, when stretched in the course direction, R_c increases as both P and n decrease because the loops separate from each other.[23]

$$R_c = \frac{\rho}{2}\sqrt{\frac{\pi H}{nP}} \quad (9)$$

Geometrical change is considered to be the main underlying mechanism in capacitive textile-based strain sensors. For instance, in agreement with the theoretical prediction (eqn (8)), the change in the capacitance of NTS@rubber@NTS@fiber sensors was observed to be linearly proportional to the change in fiber's length.[29,83] Here, the thickness of the rubber layer decreased with stretching to maintain its volume. Interestingly, the strain dependence of fiber resistance only affected the RC time constant of the capacitor and did not influence the capacitance.[83] Similar behavior was observed for double helix liquid metal core–shell fibers[32] and conductive textile/silicone elastomer/conductive textile fabric sensors (Fig. 10g)[31] in good agreement with theoretical predictions.

Textile strain sensors that sense based on the geometrical changes have shown excellent linearity, low hysteresis, high stretching–releasing cyclic stability, and large sensing range but offer limited sensitivity (GF). For instance, the NTS@rubber@NTS@fiber sensors showed linear, non-hysteretic strain sensing, large strain range of up to 950%, stable sensing response for 500 stretching–releasing cycles but with a relatively low GF of ~0.91.[29] The spring-like deformation of the coils in the coiled CNT yarn strain sensor was the likely reason for its relatively low GF (~0.13 at 25% strain).[28]

Applications

The capability of textile-based strain sensors in detecting both small and large strains has enabled their applications in monitoring microcracks formations in composites (small strains) and in detecting various movements of human body (both small and large strains) for health and sports related applications and entertainment. The following sections summarize the potential applications of textile strain sensors.

Structural health monitoring

The low sensing range of early textile strain sensor prototypes made them suitable candidates for structural health monitoring applications, which used the sensor to detect internal damages in structural materials (*e.g.* composites). It was shown that PVA/CNT fibers embedded in glass fiber reinforced composites were capable of monitoring the damages that developed

in the composite when the composite was subjected to an external load.[104] Further developments in this area brought about strain sensors made of single MWCNT coated glass fiber embedded in an epoxy matrix.[105] The electrical resistance monitored in real time showed that it detected microcracks and fracture in the composite during deformation, thereby allowing damage control.

Body movement measurements

Textile strain sensors attached to different body parts demonstrate their application in sensing small and large body movements. An early research introduced the application of PPy coated Lycra fabric strain sensor in monitoring human's knee movements.[9] By integrating a strip of the fabric sensor within a knee sleeve worn on an athlete's knee, audio feedbacks were provided to the players when the knee moved.[9] This information could be used for sports rehabilitation, sports coaching, and injury prevention. For instance, a strip of carbonized silk fabric strain sensor assembled onto a tight was used to monitor various movements of knee joints during extending, flexing, marching, jogging, jumping, and squatting.[42] By monitoring the relative changes in resistance, different motions of the knee joints could be tracked. The resistance in PEDOT-coated polyester fiber sensor embedded within a fabric knee sleeve decreased during knee movements.[37] A strip of the silver-based fabric strain sensor worn on the heel, lower knee and upper knee (Fig. 11a) to monitor heel and knee movements during activities differentiated limb movements associated with walking from other movements (Fig. 11b and c).[52]

The bending motion of an arm at different angles was monitored through a GNP-coated yarn strain sensors sewn in an elbow sleeve.[38] Relative resistance changes of the sensor allowed to locate the different arm positions. To detect closing (clenching motion) or opening (releasing motion) of the fist, a GWF/PDMS fabric based sensor was mounted on the upper arm and forearm.[41] Various finger or wrist movements have also been demonstrated in some textile sensors. For instance, a single graphite-coated silk fiber strain sensor could detect the bending movements of an index finger and wrist (Fig. 11d and e).[61] Similarly, P(VDF–TrFE) fiber sensor,[59] AgNW coated nanofiber yarn sensor,[60] and GWF/PDMS fabric based sensor[41] could detect finger's bending movements when attached to each finger using an adhesive tape. GWF/PDMS fabric sensor[41] and carbonized silk fabric strain sensor[42] were capable of monitoring wrist's bending or rotating movements. Fabric strain sensors achieved by knitted PU/PEDOT:PSS multifilaments were worn directly (without any supporting substrate or frame) on the knee, elbow, and finger, and could detect large deformation of the joints movements.[19] The fabric sensor was connected to a wireless transmitter that transferred the sensor's voltage response to a personal computer allowing remote monitoring of the user's limb movement. The voltage signal of the sensor showed a decrease when the limb was bent at an angle of 90° and increased in the straight limb position (Fig. 11f). The sensitivity and immediate responses of the knitted fabric strain sensor to the fast limb movements allowed monitoring body motion and providing feedback to the wearer corresponding to the status of their limbs.

The application of the textile strain sensors in detecting minute and subtle movements of skin associated with throat muscle during speech has also been demonstrated, which could be used in speech rehabilitation. For instance, when the rGO–PDCY yarn strain sensor was attached to the neck, it demonstrated unique current signal patterns related to the different vocalization of words such as "hi", " hello", "sensor", and "graphene".[25] Similarly, when the GNP coated yarn strain sensor was attached to a person's neck (Fig. 11g), the pattern of how the resistance changed correlated with how the words "KASIT", "PNML", "apple", and "soccer" were uttered (Fig. 11h).[38] The P(VDF–TrFE) based fiber sensor could also differentiate the words "hello", "nano" and "strain sensor" by syllable.[59] The carbonized silk fabric[42] and AgNW coated nanofiber yarn[60] strain sensors attached to the throat also produced unique signal patterns from vocalizations. As each word causes a unique movement of the vocal muscle, the pattern of the signals remained similar and unique to each word after repeating the same word.[42,60] Interestingly, the intensity of the electrical signal also changed with the strength of the syllables as demonstrated by the CPC coated PU yarn strain sensor.[45] The signal varied when the person pronounced different words such as "red", "white", "golden", "purple" and "brown". The GWF strain sensor showed that the sensing signal increased with volume when uttering different numbers, such as "one", "three", "five" and "seven" because of the increased vocal muscle movements.[65]

Textile strain sensors can also detect heart pulses to evaluate physiological conditions of the cardiovascular system for health monitoring. Textile-based heart rate monitors attached to a wrist provided the radial artery pulse waveform and systolic and diastolic peaks under normal condition[25,42,45,59,60,65] and after exercise (Fig. 11i–k).[25,42] The PVA/GNP coated NCRY[38] and carbonized silk fabric[42] strain sensors attached to the chest area were able to detect physiological changes related to respiration. A strip of carbonized silk fabric sensor attached to the chest monitored the respiration rate during relaxation or after an exercise (Fig. 11i and m).[42] Tracking the inhalation and exhalation patterns using PV/GNP coated NCRY sensor attached to the chest at each breathing cycle proved to be useful in monitoring human health conditions and identifying sleep disorders.[38] Textile strain sensors can also be used to detect tiny movements of various muscles of the human face. The carbonized silk fabric,[42] AgNW coated nanofiber yarn,[60] CPC coated PU yarn[45] and GWF[65] strain sensors attached to forehead, philtrum,[45,65] cheek or an eye's corner[42,60,65] were used to monitor facial expression and human emotions including happiness and sadness (Fig. 11n and o).

Data gloves

Data gloves are input devices with multiple strain sensors to monitor various hand movements and are widely used in robotics, virtual reality, and gesture recognition. The ability of textile strain sensors to detect various finger movements enabled the realization of new types of data gloves where soft and large-range

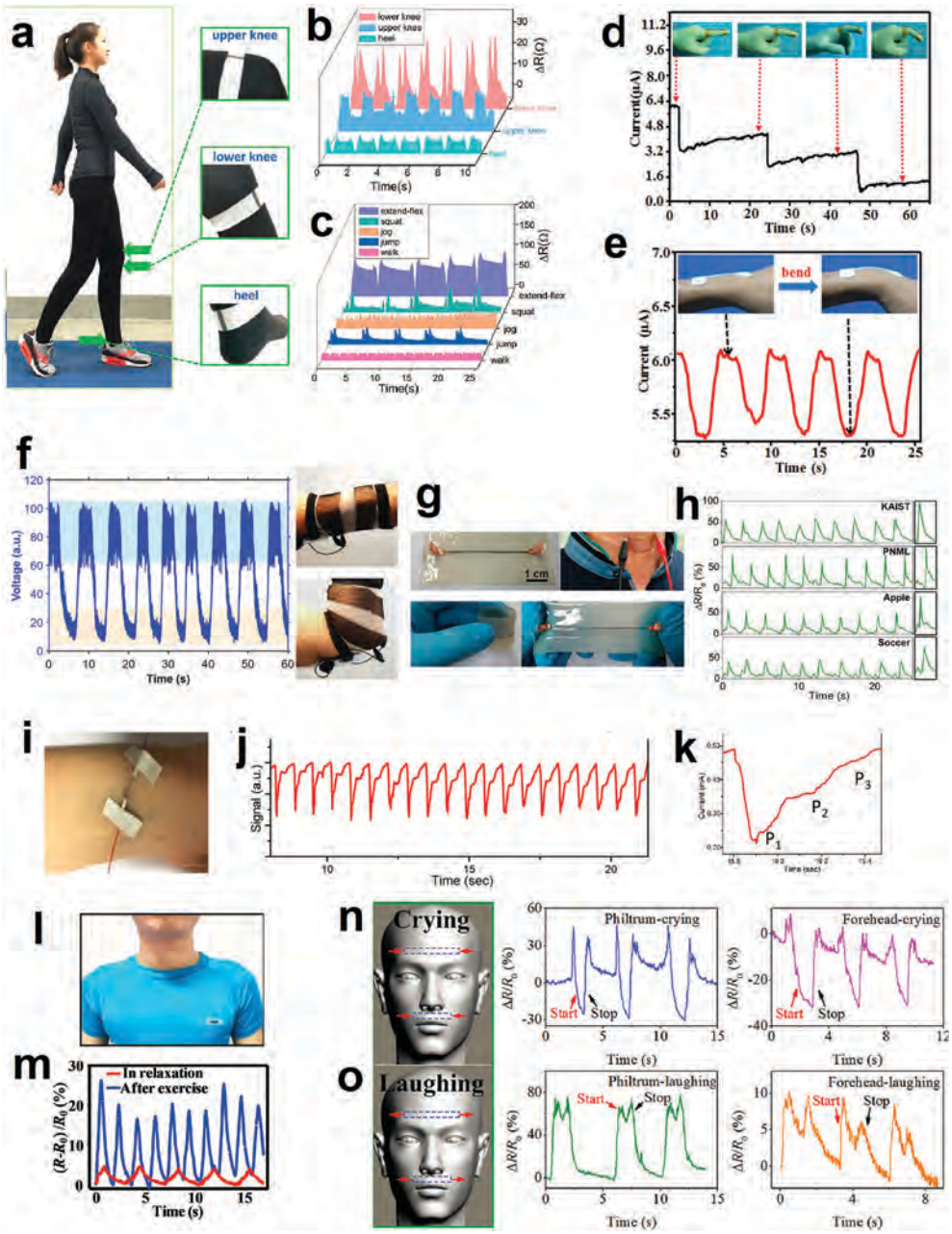

Fig. 11 (a) Photos of silver-based fabric stain sensor attached to three positions of the human body. Real-time resistance changes (b) of joints when walking, and (c) of five basic motions of the upper knee. Adapted with permission.[52] Copyright 2017 John Wiley & Sons, Inc. (d) Photo of knitted PU/PEDOT:PSS fabric strain sensor worn on a knee and its corresponding sensing signals. (e) Photo of a single graphite-coated silk fiber strain sensor attached to the index finger and the corresponding sensing signals during bending. Adapted with permission.[61] Copyright 2016 American Chemical Society. (f) Photo of a single graphite-coated silk fiber strain sensor attached to the wrist and the corresponding signals during wrist movements. Adapted with permission.[19] Copyright 2018 Elsevier Ltd. (g) Photo of PVA/GNP coated RY strain sensor embedded in an elastomeric patch attached to the neck and (h) the corresponding signals associated with muscle movements during speaking. Adapted with permission.[38] Copyright 2015 American Chemical Society. (i) Photo of AgNW-coated nanofiber yarn strain sensor attached to the wrist (j) and the corresponding sensing signal when monitoring human pulse, which shows (k) percussion (P1), tidal (P2), and diastolic (P3) waves. Adapted with permission.[60] Copyright 2017 American Chemical Society. (l) Photo of GWF strain sensor fixed on forehead and philtrum of a subject and (m) the corresponding signals of muscle motion when the subject is crying or laughing. Adapted with permission.[65] Copyright 2016 John Wiley & Sons, Inc. (n) Photo of carbonized silk fabric strain sensors attached to the chest and (o) the corresponding signals of muscle motion in relaxation and after exercise. Adapted with permission.[42] Copyright 2017 American Chemical Society.

textile sensors replaced the traditional rigid and low-range sensors. A data glove was assembled from GNP-coated WY and NCRY sensors by sewing them onto the index and middle fingers of the glove, respectively.[38] This data glove could detect simultaneous movements of the index and middle fingers. A data glove was also created by hand-weaving CPC-coated PU yarn strain sensor into every finger of a knitted glove.[45] This glove detected several hand gestures including grasping, holding,

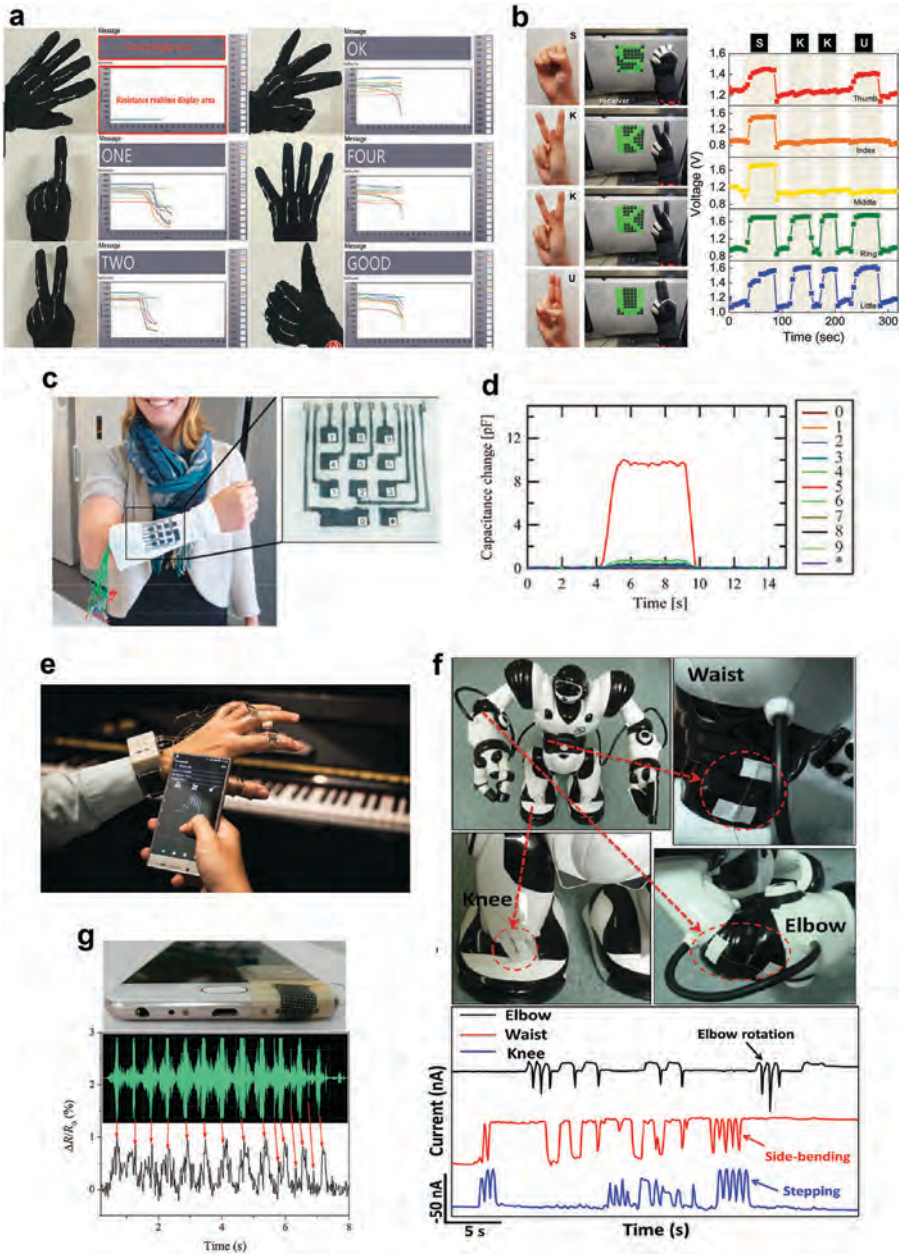

Fig. 12 (a) Photos of the data glove created by using ten independent AgNW coated P(VDF–TrFE) fiber sensors and the signals associated with different hand gestures. Adapted with permission.[59] Copyright 2016 John Wiley & Sons, Inc. (b) Photos of hand gestures when expressing different ASL letters and the output signals measured by a data glove created from PEDOT-coated PS fiber strain sensors. Adapted with permission.[37] Copyright 2017 American Chemical Society. (c) Photo of a wearable keyboard made of PEDOT:PSS-coated fabric sensor worn on arm and (d) the capacitance change when number "5" was pressed on the keyboard. Adapted with permission.[106] Copyright 2015 John Wiley & Sons, Inc. (e) Photo of wearable wireless music instrument made of GWF/PDMS sensors. Adapted with permission.[41] Copyright 2017 Royal Society of Chemistry. (f) Photos of PDCY–RGO fiber strain sensors attached to waist, knee and elbow of a robot and the corresponding signals during dancing. Adapted with permission.[25] Copyright 2015 John Wiley & Sons, Inc. (g) Photo of GWF strain sensor attached to a smart phone speaker and its signals. Adapted with permission.[65] Copyright 2017 American Chemical Society.

and releasing. A data glove assembled with five independent strips of carbonized silk fabric sensor was able to monitor real time finger bending movements.[42] A data acquisition glove system was created from ten independent AgNW coated P(VDF–TrFE) yarn sensors attached to the joint of different fingers.[59] This integrated wearable data glove system displayed different finger gestures such as "one", "two", "ok", "four", and "good" (Fig. 12a). This data glove demonstrated multilevel strain sensing based on complex representation of finger bending states such as partial bending. However, similar to the traditional prototypes, the two ends of the yarn strain sensors were fastened to an existing glove surface and were not seamlessly integrated within the glove. The utility of textile strain sensors based data gloves with multilevel sensing capability for human machine interface applications was also

demonstrated by embedding PEDOT-coated PS fiber strain sensors in each finger of a hand glove.[37] The bending and straightening movements of each finger in this case were detected by the changes in the output voltage through a voltage divider created in the glove. The data glove could identify the American sign language (ASL) letters such as "S", "K", "U", "C", and "A" when mimicked by the corresponding hand gestures (Fig. 12b). It is noteworthy that some variations in the output voltage were observed due to the changes in the resistance value at fiber interconnects. In addition, the ASL characters practiced in this study were based on static gestures while several ASL characters are dynamic.

Entertainment

Textile strain sensors are also finding applications in entertainment such as a wearable textile keyboard from a patterned PEDOT:PSS electrodes on a polyester knitted fabric.[106] This numerical textile keyboard had 10 keys (consisting of numbers from 0 to 9) and the changes in the electrode capacitance was measured by a microcontroller unit (MCU) connected to a personal computer. Upon touching each key, the capacitance of the key exceeded a certain threshold and the computer screen displayed the corresponding number. This work demonstrated that knitted fabric sensors could sense tactile inputs from human finger (Fig. 12c and d). In another work, a prototype wearable textile device integrated GWF strain sensors into a wearable musical instrument.[41] The GWF sensor embedded within a PDMS matrix made a flexible sensor that was mounted on each finger and the upper arm and then connected to a hardware device that transmitted the signals to a remote smart phone. Using a custom-built mobile application, the users could rearrange melodies to play music by motions (Fig. 12e).

Textile strain sensors worn on various body parts were used to switch LEDs that were integrated within fabrics. The feasibility was demonstrated by mounting three LEDs between two strain sensors.[65] The reversible variation in LEDs brightness was observed when the human hand was repetitively bent. The rGO–PDCY strain sensors fixed onto the waist, elbow, and knee of a robot allowed monitoring of complex movements such as dancing (Fig. 12f).[25] The use of textile strain sensor for detecting various sounds has also been demonstrated by attaching a strip of carbonized silk fabric sensor to an earphone using adhesive tape.[42] When different audio files were played, the sensor exhibited similar response to the sound wave profile. Similarly, the GWF strain sensor attached to a smart phone speaker using an adhesive tape generated sensing responses that coincided with the original audio (Fig. 12g).[65] Here, the characteristic peaks of the audio were clearly present in the sensor response.

Summary and outlook

We discussed here that it is possible to design fit-for-purpose textile sensors by implementing a combination of materials, fabrication strategies, and structural designs. Neat fiber or yarn strain sensors based on organic conductors usually possess limited stretchability (typically less than 5%) and elasticity.[48,63,107–113] Therefore, sensors made from these fibers or yarns offer a low range of strain sensing property, often up to ~1% strain, depending on their elastic deformation region.[48,63]

By coating textiles with conducting materials, it is possible to achieve mechanical properties rivalling those of the original textiles.[9] The fact that the coating does not significantly influence the stretchability of the textile substrate allows for the facile production of highly flexible and conducting stretchable textiles.[51] However, since the conducting coating layer often has significantly lower stretchability than the textile substrate, while it might be possible to operate under small deformations without significant mechanical damage,[9] large deformations often result in crack formation, leading to reduced sensing stability.[9,51,58] Further, since the surface of the textile is coated with a layer of relatively rigid conductive material, the feel of the fabric, comfort, and wearability may be different. Low environmental stability can also be a problem due to the surface of the conducting layer being exposed to the atmosphere.[9,39,49,51]

Fibers or yarns are the preferred forms of textile strain sensors since they can be easily converted into fabrics or be integrated within conventional fabrics by using textile manufacturing techniques such as weaving or knitting.[47] These formats allow for the fabrication of fabrics with highly customized patterns where traditional and sensor fibers or yarns are manipulated to achieve the desired sensing performance and/or wearability. Composite fiber processing is a popular and facile approach in fabricating individual fibers with strain sensing capability. In composite systems, because of the incorporation of the conducting component within the fiber or yarn, the properties of the host fiber such as its feel, comfort, and wearability can be greatly preserved.[24,114] Further, a higher structural integrity is expected for composite fibers or yarns compared to the coated textiles and the formation of surface microcracks that occurs in coated textiles[9,51,58] can be mitigated. As the result of the conducting component being encapsulated within the polymeric host, the conducting elastomeric fibers or yarns based strain sensors may also present higher stability than those achieved by coating approaches. However, the fabrication of these fibers or yarns can be challenging as there are a number of technical difficulties in the preparation of a spinnable composite formulation from an elastomeric host and a filler. This approach requires high quality, low particle size, and aggregate-free dispersion of fillers at high concentrations. Further, uniform and homogeneous distribution of the filler particles inside the elastomeric host is critical. However, even when these conditions are met, it does not guarantee that the fibers or yarns are suitable for strain sensing applications. Some factors that can refrain them from being used in strain sensors are as follows: in composites, a layer of polymer covers the filler. This thin coating layer can prevent the filler contact resulting in low electrical properties and high percolation thresholds.[115,116] On the other hand, some levels of interactions between the filler particles and the elastomer are required for maintaining the mechanical properties of the composite. While a significant reinforcement in stiffness can be achieved,

the integration of fillers within an elastomeric host may compromise the tensile strength and the elongation at break.[117–120] These issues must be addressed in order for the elastomeric composite fibers or yarns to become suitable for strain sensing applications.

Fiber or yarn strain sensors made using the geometrical manipulation approach such as wrapping, buckling, twisting, and coiling typically lead to high cyclic stability, which are desirable for practical applications. However, these sensors often possess low sensitivity and limited sensing range. Moreover, theses sensors are typically fabricated in centimeter scale. Sensors with high sensing range and high cyclic stability can be made from fibers with core–shell structures. Further advances in improving the sensitivity and scaling up the fabrication process of the core–shell fibers are needed.

A considerable body of research has been put forward to developing textile strain sensors that enjoy a combination of high stretchability, large-range sensing, and high sensitivity (GF). Achieving high linearity in sensing response and low hysteresis and long-term cyclic stability is also crucially important from the practical standpoint. When worn, textiles can be subjected to extremely high number of stretching–releasing deformations. Thus, researchers should show that their textile strain sensors can reliably work when cyclically stretched and released for over 100 000 cycles. There are only a few works that have demonstrated such high cyclic performance.[21,53]

Significant advancements have been achieved in terms of fabrication, understanding the sensing mechanism, and applications of resistive textile strain sensors. This is because resistive strain sensors are made of only one conducting textile electrode and are thus easy to fabricate through a variety of approaches such as coating, composite fiber spinning, geometrical manipulation (*e.g.* wrapping and coiling), and knitting. A diverse range of conducting materials such as conducting polymers (*e.g.* PANI, PPy, P3HT, and PEDOT:PSS), carbon-based materials (*e.g.* CB, CNT, graphite, and graphene) and metallic conductors (*e.g.* AgNP, AgNW, and LMs) have been used in fabricating resistive textile strain sensors. It is necessary that the textile possesses sufficient electrical conductivity that allows resistance measurements throughout the stretching and releasing deformations. Here, the changes in resistance emanates from crack formation (coating), changes in conduction network (composite), and/or geometrical transformations (wrapping, coiling, and knitting). Resistive textile strain sensors offer large-range sensing and high sensitivity, making them popular choice for wearable applications. Future research should focus on improving the linearity of their sensing response as well as on enhancing their stability and decreasing their hysteresis in long-term stretching–releasing cyclic deformations.

In contrast, capacitive textile strain sensors are more challenging to fabricate as they require two conductive textile electrodes and a dielectric layer. Buckling, coaxial fiber spinning, and knitting are the main fabrication methods for capacitive textile strain sensors. While conductivity is required in each electrode, the capacitance response is largely independent of the changes in resistance of the textile electrode during stretching and releasing. Capacitive textile strain sensors therefore offer high linearity, low hysteresis, and long-term cyclic stability, which are critical for practical applications; however, they have relatively low sensitivity and limited sensing range. More research is needed for the facile fabrication of capacitive textile strain sensors and for improving their sensitivity and sensing range. Additionally, researchers have been mainly using dielectric layers that are impermeable. For wearable applications, it is desirable that the dielectric layer is also textile based or has high permittivity. Research on textile strain sensors other than resistive and capacitive is in its infancy. More investigations are required to assess their fabrication, sensing mechanism, and suitability for textile-based applications.

Wearable applications demand that textile strain sensors be incorporated into fabrics and garments that could be comfortably worn similar to everyday clothing. While the potential integration of textile sensors with fabrics have been demonstrated, these prototypes were made by manual stitching the sensor on every-day apparels, by mounting a small piece of textile sensors on an elastic substrate, or by using specially-designed and bulky supporting frames.[16,17,21,71] The comfort attributes and appeal of wearable strain sensors for mass use will be achieved once the textile sensor can be directly worn without the need for a supporting frame, substrate, or an additional clothing item. A recent work demonstrated the production of conductive elastomeric multifilaments in kilometer scale. These fibers were knitted into fabrics that could be directly worn on various body parts (*e.g.* knee, elbow, and finger) without the need for any supporting structures or frames.[19,20] The strain sensing behavior of the fabric was modulated using various loop configurations and stitch insertions in the knit structures. This strategy is appealing for manipulating the strain sensing property on a fabric level to match the comfort attributes required from a wearable smart clothing.

Another challenge in practical application of textile strain sensors is the establishing of effective communication between the sensor and other electronics (*e.g.* to a wireless transmitter). Metallic interconnects are the present standard, which are not particularly appealing and practical. Combined advances in electronics, software, and textile manufacture are required to achieve effective transmission of the sensing signal to a personal computing device. The application software should be able to undertake analysis of sensing signals and provide useful feedback to the user or wearer as required. In addition, the textile strain sensor and the electrical equipment to which it is connected may need power to operate for certain period. Since conventional power sources such as batteries are rigid, advances in wearable energy storage alternatives[121–124] that can be readily incorporated with the fabric and provide sufficient power for the function of the textile strain sensor are also necessary. These wearable power sources should ideally be stretchable[125] to withstand the large strains applied to the fabric during its normal use.

Finally, it is important to recognize that each application demands for specific sensing requirements. The enhanced capability of present textile sensors in detecting both small to

large deformations and also a range of motions from extension to torsions, have opened the doors for diverse applications. Here, we have summarized some applications in structural health monitoring, body movement measurements, data gloves, and entertainment. However, other applications remain relatively less explored. Because of their flexibility and wearability, textile strain sensors can serve as suitable platforms for applications in therapeutics, remote medical health monitoring,[11–14] virtual reality, and robotics.[6] For instance, textile sensors can enable biomechanical analysis for continuous monitoring of body kinematics and vital signs.[24]

Conflicts of interest

There are no conflicts to declare.

Acknowledgements

The authors acknowledge financial support from the Australian Research Council (FT130100380, IH140100018, and DP170102859), Institute for Frontier Materials (Impact Grant), and Deakin University (Alfred Deakin Postdoctoral Research Fellowship).

References

1 A. L. Window, *Strain Gauge Technology*, Springer, 2nd edn, 1993.
2 P. C. Chang, A. Flatau and S. C. Liu, *Struct. Health Monit.*, 2003, **2**, 257–267.
3 D. Barke and W. K. Chiu, *Struct. Health Monit.*, 2005, **4**, 81–94.
4 F. Lorussi, E. P. Scilingo, M. Tesconi, A. Tognetti and D. De Rossi, *IEEE Trans. Inf. Technol. Biomed.*, 2005, **9**, 372–381.
5 C. Mattmann, F. Clemens and G. Tröster, *Sensors*, 2008, **8**, 3719–3732.
6 T. Yamada, Y. Hayamizu, Y. Yamamoto, Y. Yomogida, A. Izadi-Najafabadi, D. N. Futaba and K. Hata, *Nat. Nanotechnol.*, 2011, **6**, 296–301.
7 Y. Wang, L. Wang, T. Yang, X. Li, X. Zang, M. Zhu, K. Wang, D. Wu and H. Zhu, *Adv. Funct. Mater.*, 2014, **24**, 4666–4670.
8 P. T. Gibbs and H. H. Asada, *J. Neuroeng. Rehabil.*, 2005, **2**, 7.
9 J. Wu, D. Zhou, C. O. Too and G. G. Wallace, *Synth. Met.*, 2005, **155**, 698–701.
10 B. J. Munro, T. E. Campbell, G. G. Wallace and J. R. Steele, *Sens. Actuators, B*, 2008, **131**, 541–547.
11 F. Carpi, D. DeRossi and D. De Rossi, *IEEE Trans. Inf. Technol. Biomed.*, 2005, **9**, 295–318.
12 A. Lymberis and S. Olsson, *Telemed. J. e-Health*, 2003, **9**, 379–386.
13 H. D. Kubo and B. C. Hill, *Phys. Med. Biol.*, 1996, **41**, 83–91.
14 S. Majumder, T. Mondal and M. Deen, *Sensors*, 2017, **17**, 130.
15 J. Wang, P. Xue, X. Tao and T. Yu, *Adv. Eng. Mater.*, 2014, **16**, 565–570.
16 S. Seyedin, J. M. Razal, P. C. Innis, A. Jeiranikhameneh, S. Beirne and G. G. Wallace, *ACS Appl. Mater. Interfaces*, 2015, **7**, 21150–21158.
17 J. Foroughi, G. M. Spinks, S. Aziz, A. Mirabedini, A. Jeiranikhameneh, G. G. Wallace, M. E. Kozlov and R. H. Baughman, *ACS Nano*, 2016, **10**, 9129–9135.
18 G. Cai, M. Yang, Z. Xu, J. Liu, B. Tang and X. Wang, *Chem. Eng. J.*, 2017, **325**, 396–403.
19 S. Seyedin, S. Moradi, C. Singh and J. M. Razal, *Appl. Mater. Today*, 2018, **11**, 255–263.
20 S. Seyedin, S. Moradi, C. Singh and J. M. Razal, *Data Brief*, 2018, **18**, 1765–1772.
21 Z. Wang, Y. Huang, J. Sun, Y. Huang, H. Hu, R. Jiang, W. Gai, G. Li and C. Zhi, *ACS Appl. Mater. Interfaces*, 2016, **8**, 24837–24843.
22 R. Wang, N. Jiang, J. Su, Q. Yin, Y. Zhang, Z. Liu, H. Lin, F. A. Moura, N. Yuan, S. Roth, R. S. Rome, R. Ovalle-Robles, K. Inoue, S. Yin, S. Fang, W. Wang, J. Ding, L. Shi, R. H. Baughman and Z. Liu, *Adv. Funct. Mater.*, 2017, **27**, 1702134.
23 O. Atalay and W. Kennon, *Sensors*, 2014, **14**, 4712–4730.
24 S. Coyle, Y. Wu, K. Lau, D. De Rossi, G. Wallace and D. Diamond, *MRS Bull.*, 2007, **32**, 434–442.
25 Y. Cheng, R. Wang, J. Sun and L. Gao, *Adv. Mater.*, 2015, **27**, 7365–7371.
26 M. Zhang, C. Wang, H. Wang, M. Jian, X. Hao and Y. Zhang, *Adv. Funct. Mater.*, 2017, **27**, 1604795.
27 M. Z. Seyedin, J. M. Razal, P. C. Innis and G. G. Wallace, *Adv. Funct. Mater.*, 2014, **24**, 2957–2966.
28 Y. Shang, Y. Li, X. He, L. Zhang, Z. Li, P. Li, E. Shi, S. Wu and A. Cao, *Nanoscale*, 2013, **5**, 2403–2410.
29 Z. F. Liu, S. Fang, F. A. Moura, J. N. Ding, N. Jiang, J. Di, M. Zhang, X. Lepro, D. S. Galvao, C. S. Haines, N. Y. Yuan, S. G. Yin, D. W. Lee, R. Wang, H. Y. Wang, W. Lv, C. Dong, R. C. Zhang, M. J. Chen, Q. Yin, Y. T. Chong, R. Zhang, X. Wang, M. D. Lima, R. Ovalle-Robles, D. Qian, H. Lu and R. H. Baughman, *Science*, 2015, **349**, 400–404.
30 C. Choi, J. M. Lee, S. H. Kim, S. J. Kim, J. Di and R. H. Baughman, *Nano Lett.*, 2016, **16**, 7677–7684.
31 A. Atalay, V. Sanchez, O. Atalay, D. M. Vogt, F. Haufe, R. J. Wood and C. J. Walsh, *Adv. Mater. Technol.*, 2017, **2**, 1700136.
32 C. B. Cooper, K. Arutselvan, Y. Liu, D. Armstrong, Y. Lin, M. R. Khan, J. Genzer and M. D. Dickey, *Adv. Funct. Mater.*, 2017, **27**, 1605630.
33 Q. Liao, M. Mohr, X. Zhang, Z. Zhang, Y. Zhang and H.-J. Fecht, *Nanoscale*, 2013, **5**, 12350.
34 H. J. Sim, C. Choi, C. J. Lee, Y. T. Kim, G. M. Spinks, M. D. Lima, R. H. Baughman and S. J. Kim, *Adv. Eng. Mater.*, 2015, **17**, 1270–1275.
35 J. Zhong, Q. Zhong, Q. Hu, N. Wu, W. Li, B. Wang, B. Hu and J. Zhou, *Adv. Funct. Mater.*, 2015, **25**, 1798–1803.
36 D. Graham-Rowe, *Nat. Photonics*, 2007, **1**, 307–309.
37 J. Eom, R. Jaisutti, H. Lee, W. Lee, J.-S. Heo, J.-Y. Lee, S. K. Park and Y.-H. Kim, *ACS Appl. Mater. Interfaces*, 2017, **9**, 10190–10197.

38 J. J. Park, W. J. Hyun, S. C. Mun, Y. T. Park and O. O. Park, *ACS Appl. Mater. Interfaces*, 2015, **7**, 6317–6324.
39 C. Cochrane, V. Koncar, M. Lewandowski and C. Dufour, *Sensors*, 2007, **7**, 473–492.
40 X. Li, P. Sun, L. Fan, M. Zhu, K. Wang, M. Zhong, J. Wei, D. Wu, Y. Cheng and H. Zhu, *Sci. Rep.*, 2012, **2**, 395.
41 X. Liu, C. Tang, X. Du, S. Xiong, S. Xi, Y. Liu, X. Shen, Q. Zheng, Z. Wang, Y. Wu, A. Horner and J.-K. Kim, *Mater. Horiz.*, 2017, **4**, 477–486.
42 C. Wang, X. Li, E. Gao, M. Jian, K. Xia, Q. Wang, Z. Xu, T. Ren and Y. Zhang, *Adv. Mater.*, 2016, **28**, 6640–6648.
43 S. Ryu, P. Lee, J. B. Chou, R. Xu, R. Zhao, A. J. Hart and S.-G. Kim, *ACS Nano*, 2015, **9**, 5929–5936.
44 T. Lee, W. Lee, S.-W. Kim, J. J. Kim and B.-S. Kim, *Adv. Funct. Mater.*, 2016, **26**, 6206–6214.
45 X. Wu, Y. Han, X. Zhang and C. Lu, *ACS Appl. Mater. Interfaces*, 2016, **8**, 9936–9945.
46 A. J. Granero, P. Wagner, K. Wagner, J. M. Razal, G. G. Wallace and M. in het Panhuis, *Adv. Funct. Mater.*, 2011, **21**, 955–962.
47 R. Zhang, H. Deng, R. Valenca, J. Jin, Q. Fu, E. Bilotti and T. Peijs, *Sens. Actuators, A*, 2012, **179**, 83–91.
48 H. Zhao, Y. Zhang, P. D. Bradford, Q. Zhou, Q. Jia, F.-G. Yuan and Y. Zhu, *Nanotechnology*, 2010, **21**, 305502.
49 Y. Li, X. Y. Cheng, M. Y. Leung, J. Tsang, X. M. Tao and M. C. W. Yuen, *Synth. Met.*, 2005, **155**, 89–94.
50 K. W. Oh, H. J. Park and S. H. Kim, *J. Appl. Polym. Sci.*, 2003, **88**, 1225–1229.
51 Y. Ding, M. A. Invernale and G. A. Sotzing, *ACS Appl. Mater. Interfaces*, 2010, **2**, 1588–1593.
52 Y. Li, Y. Li, M. Su, W. Li, Y. Li, H. Li, X. Qian, X. Zhang, F. Li and Y. Song, *Adv. Electron. Mater.*, 2017, **3**, 1700253.
53 S. J. Kim, W. Song, Y. Yi, B. K. Min, S. Mondal, K.-S. An and C.-G. Choi, *ACS Appl. Mater. Interfaces*, 2018, **10**, 3921–3928.
54 C. Robert, J. F. Feller and M. Castro, *ACS Appl. Mater. Interfaces*, 2012, **4**, 3508–3516.
55 J. Ren, C. Wang, X. Zhang, T. Carey, K. Chen, Y. Yin and F. Torrisi, *Carbon*, 2017, **111**, 622–630.
56 P. Calvert, D. Duggal, P. Patra, A. Agrawal and A. Sawhney, *Mol. Cryst. Liq. Cryst.*, 2008, **484**, 291–302.
57 Q. Fan, X. Zhang and Z. Qin, *J. Macromol. Sci., Part B: Phys.*, 2012, **51**, 736–746.
58 J. P. Wang, P. Xue and X. M. Tao, *Mater. Sci. Eng., A*, 2011, **528**, 2863–2869.
59 S. Chen, Z. Lou, D. Chen, K. Jiang and G. Shen, *Adv. Mater. Technol.*, 2016, **1**, 1600136.
60 W. Zhong, C. Liu, C. Xiang, Y. Jin, M. Li, K. Liu, Q. Liu, Y. Wang, G. Sun and D. Wang, *ACS Appl. Mater. Interfaces*, 2017, **9**, 42058–42066.
61 M. Zhang, C. Wang, Q. Wang, M. Jian and Y. Zhang, *ACS Appl. Mater. Interfaces*, 2016, **8**, 20894–20899.
62 X. Liao, Q. Liao, Z. Zhang, X. Yan, Q. Liang, Q. Wang, M. Li and Y. Zhang, *Adv. Funct. Mater.*, 2016, **26**, 3074–3081.
63 X. Wang, X. Fu and D. D. L. Chung, *J. Mater. Res.*, 1999, **14**, 790–802.
64 A. Lekawa-Raus, K. K. K. Koziol and A. H. Windle, *ACS Nano*, 2014, **8**, 11214–11224.
65 B. Yin, Y. Wen, T. Hong, Z. Xie, G. Yuan, Q. Ji and H. Jia, *ACS Appl. Mater. Interfaces*, 2017, **9**, 32054–32064.
66 E. Bilotti, R. Zhang, H. Deng, M. Baxendale and T. Peijs, *J. Mater. Chem.*, 2010, **20**, 9449–9455.
67 J. R. Bautista-Quijano, P. Pötschke, H. Brünig and G. Heinrich, *Polymer*, 2016, **82**, 181–189.
68 P. Sukitpaneenit, T. Thanpitcha, A. Sirivat, C. Weder and R. Rujiravanit, *J. Appl. Polym. Sci.*, 2007, **106**, 4038–4046.
69 M. Z. Seyedin, J. M. Razal, P. C. Innis, R. Jalili and G. G. Wallace, *Adv. Funct. Mater.*, 2015, **25**, 94–104.
70 S. Seyedin, J. M. Razal, P. C. Innis and G. G. Wallace, *Smart Mater. Struct.*, 2016, **25**, 035015.
71 S. Lee, S. Shin, S. Lee, J. Seo, J. Lee, S. Son, H. J. Cho, H. Algadi, S. Al-Sayari, D. E. Kim and T. Lee, *Adv. Funct. Mater.*, 2015, **25**, 3114–3121.
72 Y. Lu, J. Jiang, S. Yoon, K.-S. Kim, J.-H. Kim, S. Park, S.-H. Kim and L. Piao, *ACS Appl. Mater. Interfaces*, 2018, **10**, 2093–2104.
73 A. J. Granero, J. M. Razal, G. G. Wallace and M. in het Panhuis, *2010 International Conference on Nanoscience and Nanotechnology*, IEEE, Sydney, 2010, pp. 80–83.
74 Y. Wei, S. Chen, X. Yuan, P. Wang and L. Liu, *Adv. Funct. Mater.*, 2016, **26**, 5078–5085.
75 Y. Shang, X. He, Y. Li, L. Zhang, Z. Li, C. Ji, E. Shi, P. Li, K. Zhu, Q. Peng, C. Wang, X. Zhang, R. Wang, J. Wei, K. Wang, H. Zhu, D. Wu and A. Cao, *Adv. Mater.*, 2012, **24**, 2896–2900.
76 Y. Li, Y. Shang, X. He, Q. Peng, S. Du, E. Shi, S. Wu, Z. Li, P. Li and A. Cao, *ACS Nano*, 2013, **7**, 8128–8135.
77 S. Zhu, J. H. So, R. Mays, S. Desai, W. R. Barnes, B. Pourdeyhimi and M. D. Dickey, *Adv. Funct. Mater.*, 2013, **23**, 2308–2314.
78 Y. Wu, R. Zhen, H. Liu, S. Liu, Z. Deng, P. Wang, S. Chen and L. Liu, *J. Mater. Chem. C*, 2017, **5**, 12483–12491.
79 X. Wang, Y. Qiu, W. Cao and P. Hu, *Chem. Mater.*, 2015, **27**, 6969–6975.
80 Z. Tang, S. Jia, F. Wang, C. Bian, Y. Chen, Y. Wang and B. Li, *ACS Appl. Mater. Interfaces*, 2018, **10**, 6624–6635.
81 J. Zhou, X. Xu, Y. Xin and G. Lubineau, *Adv. Funct. Mater.*, 2018, **28**, 1705591.
82 S. Chen, H. Liu, S. Liu, P. Wang, S. Zeng, L. Sun and L. Liu, *ACS Appl. Mater. Interfaces*, 2018, **10**, 4305–4314.
83 H. Wang, Z. Liu, J. Ding, X. Lepró, S. Fang, N. Jiang, N. Yuan, R. Wang, Q. Yin, W. Lv, Z. Liu, M. Zhang, R. Ovalle-Robles, K. Inoue, S. Yin and R. H. Baughman, *Adv. Mater.*, 2016, **28**, 4998–5007.
84 A. Frutiger, J. T. Muth, D. M. Vogt, Y. Mengüç, A. Campo, A. D. Valentine, C. J. Walsh and J. A. Lewis, *Adv. Mater.*, 2015, **27**, 2440–2446.
85 Y.-L. Li, I. A. Kinloch and A. H. Windle, *Science*, 2004, **304**, 276–278.
86 S. Seyedin, J. M. Razal, P. C. Innis, R. Jalili and G. G. Wallace, *Adv. Mater. Interfaces*, 2016, **3**, 1500672.
87 D.-Y. Khang, H. Jiang, Y. Huang and J. A. Rogers, *Science*, 2006, **311**, 208–212.

88 G. M. Whitesides, N. Bowden, S. Brittain, A. G. Evans and J. W. Hutchinson, *Nature*, 1998, **393**, 146–149.
89 S. Y. Yang, K. H. Cho, Y. Kim, M.-G. Song, H. S. Jung, J. W. Yoo, H. Moon, J. C. Koo, J. Nam and H. R. Choi, *Smart Mater. Struct.*, 2017, **26**, 105025.
90 M. Hiraoka, K. Nakamura, H. Arase, K. Asai, Y. Kaneko, S. W. John, K. Tagashira and A. Omote, *Sci. Rep.*, 2016, **6**, 36358.
91 Y. Shang, Y. Li, X. He, S. Du, L. Zhang, E. Shi, S. Wu, Z. Li, P. Li, J. Wei, K. Wang, H. Zhu, D. Wu and A. Cao, *ACS Nano*, 2013, **7**, 1446–1453.
92 H. Zhang, X. Tao, T. Yu and S. Wang, *Sens. Actuators, A*, 2006, **126**, 129–140.
93 Y. Zhou, J. He, H. Wang, K. Qi, N. Nan, X. You, W. Shao, L. Wang, B. Ding and S. Cui, *Sci. Rep.*, 2017, **7**, 1–9.
94 Y. Tajitsu, Y. Kawase, K. Katsuya, M. Tamura, K. Sakamoto, K. Kawahara, Y. Harada, T. Kondo and Y. Imada, *IEEE Trans. Dielectr. Electr. Insul.*, 2018, **25**, 772–777.
95 J. Cao, Q. Wang and H. Dai, *Phys. Rev. Lett.*, 2003, **90**, 157601.
96 P. Xue, X. M. Tao and H. Y. Tsang, *Appl. Surf. Sci.*, 2007, **253**, 3387–3392.
97 X. Li, T. Hua and B. Xu, *Carbon*, 2017, **118**, 686–698.
98 Y. Cheng, R. Wang, H. Zhai and J. Sun, *Nanoscale*, 2017, **9**, 3834–3842.
99 X. Li, R. Zhang, W. Yu, K. Wang, J. Wei, D. Wu, A. Cao, Z. Li, Y. Cheng, Q. Zheng, R. S. Ruoff and H. Zhu, *Sci. Rep.*, 2012, **2**, 870.
100 M. Zahid, E. L. Papadopoulou, A. Athanassiou and I. S. Bayer, *Mater. Des.*, 2017, **135**, 213–222.
101 D. Stauffer and A. Aharony, *Introduction to Percolation Theory*, CRC Press, London, 2nd edn, 1994.
102 L. Li, W. M. Au, K. M. Wan, S. H. Wan, W. Y. Chung and K. S. Wong, *Text. Res. J.*, 2010, **80**, 935–947.
103 R. Holm, *Electric Contacts: Theory and Applications*, Springer, New York, 4th edn, 1967.
104 N. D. Alexopoulos, C. Bartholome, P. Poulin and Z. Marioli-Riga, *Compos. Sci. Technol.*, 2010, **70**, 1733–1741.
105 J. Zhang, J. Liu, R. Zhuang, E. Mäder, G. Heinrich and S. Gao, *Adv. Mater.*, 2011, **23**, 3392–3397.
106 S. Takamatsu, T. Lonjaret, E. Ismailova, A. Masuda, T. Itoh and G. G. Malliaras, *Adv. Mater.*, 2016, **28**, 4485–4488.
107 L. M. Ericson, H. Fan, H. Peng, V. A. Davis, W. Zhou, J. Sulpizio, Y. Wang, R. Booker, J. Vavro, C. Guthy, A. N. G. Parra-Vasquez, M. J. Kim, S. Ramesh, R. K. Saini, C. Kittrell, G. Lavin, H. Schmidt, W. W. Adams, W. E. Billups, M. Pasquali, W.-F. Hwang, R. H. Hauge, J. E. Fischer and R. E. Smalley, *Science*, 2004, **305**, 1447–1450.
108 G. M. Spinks, V. Mottaghitalab, M. Bahrami-Samani, P. G. Whitten and G. G. Wallace, *Adv. Mater.*, 2006, **18**, 637–640.
109 J. Foroughi, G. M. Spinks, G. G. Wallace and P. G. Whitten, *Synth. Met.*, 2008, **158**, 104–107.
110 R. Jalili, J. M. Razal, P. C. Innis and G. G. Wallace, *Adv. Funct. Mater.*, 2011, **21**, 3363–3370.
111 Z. Xu and C. Gao, *Nat. Commun.*, 2011, **2**, 571.
112 Z. Dong, C. Jiang, H. Cheng, Y. Zhao, G. Shi, L. Jiang and L. Qu, *Adv. Mater.*, 2012, **24**, 1856–1861.
113 Z. Xu, H. Sun, X. Zhao and C. Gao, *Adv. Mater.*, 2013, **25**, 188–193.
114 D. Zou, Z. Lv, X. Cai and S. Hou, *Nano Energy*, 2012, **1**, 273–281.
115 K. Yurekli, R. Krishnamoorti, M. F. Tse, K. O. McElrath, A. H. Tsou and H.-C. Wang, *J. Polym. Sci., Part B: Polym. Phys.*, 2001, **39**, 256–275.
116 W. Bauhofer and J. Z. Kovacs, *Compos. Sci. Technol.*, 2009, **69**, 1486–1498.
117 F. M. Blighe, W. J. Blau and J. N. Coleman, *Nanotechnology*, 2008, **19**, 415709.
118 U. Khan, F. M. Blighe and J. N. Coleman, *J. Phys. Chem. C*, 2010, **114**, 11401–11408.
119 U. Khan, P. May, A. O'Neill and J. N. Coleman, *Carbon*, 2010, **48**, 4035–4041.
120 B. Fernández-d'Arlas, U. Khan, L. Rueda, J. N. Coleman, I. Mondragon, M. A. Corcuera and A. Eceiza, *Compos. Sci. Technol.*, 2011, **71**, 1030–1038.
121 K. Jost, G. Dion and Y. Gogotsi, *J. Mater. Chem. A*, 2014, **2**, 10776–10787.
122 D. Yu, Q. Qian, L. Wei, W. Jiang, K. Goh, J. Wei, J. Zhang and Y. Chen, *Chem. Soc. Rev.*, 2015, **44**, 647–662.
123 S. Seyedin, E. R. S. Yanza and J. M. Razal, *J. Mater. Chem. A*, 2017, **5**, 24076–24082.
124 J. Zhang, S. Seyedin, Z. Gu, W. Yang, X. Wang and J. M. Razal, *Nanoscale*, 2017, **9**, 18604–18608.
125 S. Qin, S. Seyedin, J. Zhang, Z. Wang, F. Yang, Y. Liu, J. Chen and J. M. Razal, *Macromol. Rapid Commun.*, 2018, **39**, 1800103.
126 A. Mirabedini, J. Foroughi and G. G. Wallace, *RSC Adv.*, 2016, **6**, 44687–44716.